2. EXPLANATORY NOTES

RESPONSIBILITIES FOR AUTHORSHIP

In contrast to previous volumes of the *Initial Reports*, the decision was made for this report that there should not be a division into Shipboard Site Reports and Shore Laboratory Studies. Rather, it was thought desirable to concentrate into the site chapters all the primary data referring to one site, whether studied on board or ashore by members of the shipboard scientific party, or whether studied by the numerous colleagues who have co-operated with the drilling project in specialized aspects of the cores. In this way all relevant data are collected together in one place before the discussion and interpretation of the results are presented. The authorship of the site chapters is collectively the shipboard scientific party, the ultimate responsibility lying with the two co-chief scientists. However in order to give due credit to work of those colleagues not on board who have contributed data and interpretations, their names are given at the head of the appropriate section in the text.

Chapters 3 to 10 present the data and discussions on the sites where holes have been drilled. Each chapter follows the same pattern: The first two sections give the site background and objectives, and survey data, and have been written by A. S. Laughton (except Site 111, which is by A. S. Ruffman). Sections on drilling characteristics were written by A. S. Laughton, sections on lithology were written by T. A. Davies, U. A. Franz and L. F. Musich, sections on physical properties were written by R. B. Whitmarsh, sections on paleontology and sedimentation rates were written by W. A. Berggren, R. N. Benson, J. E. van Hinte and K. A. Perch-Nielsen, and the discussion sections by A. S. Laughton (except for Site 111 which is by A. S. Ruffman).

A general summary of all the holes and a discussion of various aspects of results common to all holes or to groups of holes in various regions are presented in Chapters 11 to 21. The authorship of these chapters, many of which are more speculative than the previous chapters, is indicated in the text.

SURVEY DATA

Only two detailed site surveys had been made prior to the start of Leg 12. One was at a site in Rockall Trough which was not drilled. The other in the Hatton-Rockall Basin was made by *Discovery* Cruise 33 in April, 1970. An account of the site survey is given in Appendix II.

Short surveys were made on *Glomar Challenger* before laying the beacon, using a precision echo-sounder, seismic profiler and magnetometer.

All depth measurements by sonic methods have utilized a Gifft precision graphic recorder. Uncorrected depths (in fathoms) are measured from the recordings assuming a full scale of 400 fathoms for a one-second sweep. Corrected depths (in meters) have been adjusted for: (a) actual speed-of-sound in water from Matthews (1939) tables, and (b) actual depth of the echo-sounding transducer below water level, assumed constant at 6 meters.

In addition, any depths or distances referred to the drilling platform have been calculated under the assumption that this level is 10 meters above the water line. The water depths cited for each hole were usually determined from the echo-sounder since it was seldom possible to feel the bottom with the drill pipe.

Seismic profiles were made using two Bolt airguns simultaneously (5 cu. in. and 20 cu. in.), a Scripps designed hydrophone streamer and two Edo recorders, usually recording at two different filter settings (80-160 Hz and 160-320 Hz, or later 40-80 Hz and 80-160 Hz).

Magnetic field measurements were made with a Varian proton magnetometer.

On passage between sites, continuous observations were made of depth, magnetic field and subbottom structure, although it was not possible to spare the time to obtain a better seismic record by steaming at less than cruising speed. The geophysical data obtained on passage is presented in Appendix III.

During the first two and a half weeks, the navigation was controlled by a satellite navigator. This, however, broke down and we were unable to obtain on-line fixes throughout the rest of Leg 12. However after twelve days, the system was rigged so that satellite passes were recorded on punched tape and these fixes were calculated after the cruise at Scripps and could be used retrospectively to correct track and site positions.

After the breakdown of the satellite navigator, navigation was entirely by celestial observation with occasional Loran A fixes, making it difficult to locate the precise position to lay a beacon. The ultimate positions of Holes 114 and 115 were determined solely by celestial observations. The remainder were fixed by satellite.

BASIS FOR NUMBERING SITES, HOLES, CORES AND SECTIONS

A site number refers to a single hole or group of holes drilled in essentially the same position using the same acoustic beacon. The first hole at a site (for example, Site 111) was given the number of the site (for example, Hole 111). Second holes drilled by withdrawing from the first hole and redrilling were labeled "A" holes (Hole 111A).

A core was usually taken by dropping a core barrel down the drill string, and coring for 9 meters as measured by lowering of drill string before recovery. The sediment was retained in a plastic liner 9.28 meters long inside the core barrel, and in a 0.20 meter long core catcher assembly below the liner. The liner was not normally full.

On recovery the liner was cut into sections of 1.5 meters measured from the lowest point of sediment within the liner (Figure 1).

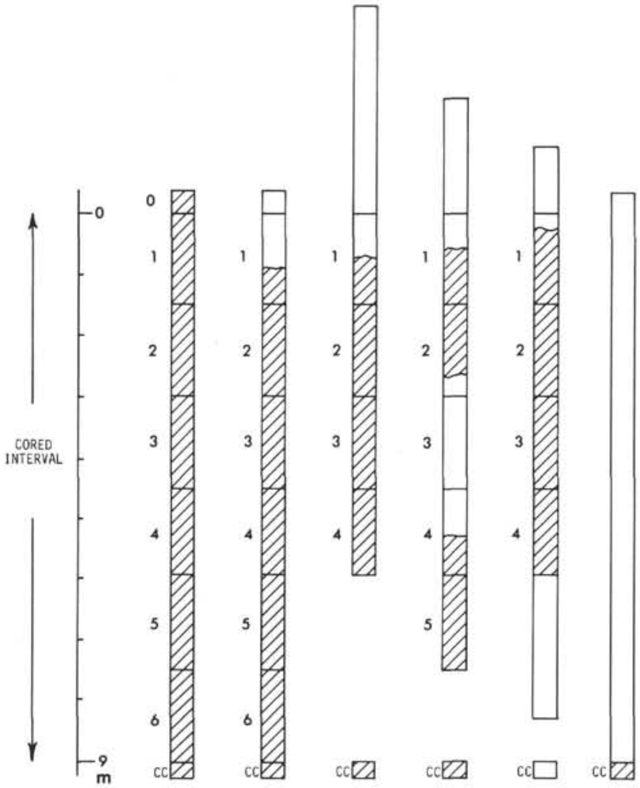

Figure 1. *The method of labeling sections of cores when recovery is complete, incomplete and divided. The cores have been lined up so that the top of Section 1 is always coincident with the top of the cored interval, according to the method of calcutating downhole depth of samples. Core catcher samples are always considered to have come from the bottom of the cored interval, regardless of the depth assigned to the adjacent section above.*

In general the top of the core did not coincide with the top of a section. The sections were labeled from 1 for the top (incomplete) section to a figure as high as 6 for the bottom (complete) section, depending on the total length of core recovered.

In the event that there were gaps in the core resulting in empty sections, these were still given numbers in sequence. Core catcher samples are always considered to have come from the bottom of the cored interval regardless of the depth assigned to the adjacent section above.

On occasions, over 9 meters of core were recovered. The small remainder was labeled Section 0 (zero) being above Section 1. On other occasions the sum of the lengths of numbered sections exceeds the total length of core recovered and also the cored interval, resulting in an overlap of nominal depth downhole of the bottom of one core and the top of the core below. In such cases a special note has been made.

(In some holes, for example, 118-12 to 15, 119-28 to 40, it was found desirable to drill with high water circulation but with a core barrel in place in order to penetrate faster. The drilled interval was often considerably greater than the 9 meters of the core barrel, the principle being that the high water circulation prevented sediments from being recovered. However, some of the harder layers were probably recovered during this procedure. It was difficult, therefore, to assign the correct depth in the hole to these sediments and each case had to be considered on its merits).

All samples taken from cores were numbered before being processed, according to the system described in the Shipboard Handbook for Leg 12. The label "12-111-3-2, 25 cm" thus refers to Leg 12, Hole 111, Core 3, Section 2, sampled 25 centimeters from the top of that section. The label "12-111-3-CC" refers to the core catcher sample at the base of Core 3.

It is appreciated that with this labeling system, the top of the core material recovered may be located at say, 1.3 meters below the top of Section 1 and the bottom will be at 1.5 meters in, say, Section 2 (if the total recovery is 1.7 meters). In relating this to downhole depths, there is an arbitrariness of several meters. However, it is impossible to assess where exactly in the hole the sample came from. Sometimes the core barrel will jam up with a hard sediment after sampling a few meters, this will then really represent the first few meters penetrated. At other times the circulation of water may wash away the upper softer part of a core and recovery will represent the lower part. Separated lengths of core in a core liner may come from the drill bit being lifted off the bottom during coring in rough sea conditions. Similarly, there is no guarantee that the core catcher sample represents the material at the base of the cored interval.

The labeling of samples is therefore rigorously tied to the position of the samples within a section as the position appears when the section is first cut open and as logged in the visual core description sheets. The section labeling system implies that the top of the core is within 1.5 meters of the top of the cored interval. Thus, the downhole depth of 12-111-3-2, 25 centimeters is calculated as follows. The top of cored interval of Core 3 is 189 meters. The top of Section 2 is 1.5 meters below top of cored interval, that is, at 190.5 meters. The sample is 25 meters below the top of Section 2, that is, at 190.75 meters.

For the purposes of presenting the data for the entire hole in the hole summary sheets where one meter is represented by less than one millimeter, the top of the recovered sediment is always drawn at the top of the cored interval. The error involved in this presentation is always less than 1.5 meters compared with depths calculated from the sample label.

HANDLING OF CORES

The first assessment of the core material was made rapidly on samples from the core catcher. An age by nannoplankton examination enabled rapid decisions to be made on whether to drill ahead or to take another core. Core catcher material was also used initially for foraminiferal and radiolarian determinations.

After a core section had been cut, sealed and labeled, it was brought into the core laboratory for processing. The routine procedure listed below was usually followed:

1. Weighing of the core section for mean bulk density measurement.

2. GRAPE analysis for bulk density.

3. Gamma ray counting for radioactivity.

4. Sonic velocity determinations, after a period of at least 4 hours for temperature equilibration. Sonic velocity was not determined for water sections. Special measurements were made on hard rock cores where the diameter was less than the core liner.

After the physical measurements were made, the core liner was cut by an electric saw, and the end caps by a knife. The core could then be split into halves by a cheese cutter, if the sediment was a soft ooze. At times, when compacted or partially lithified sediments were included, the core had to be split by a machine band saw or diamond wheel.

One of the split halves was designated a working half. Penetrometer readings were taken to give a measure of the degree of consolidation of the sediments. Samples, including those for grain size, X-ray mineralogy, interstitial water chemistry and total carbonate content, were taken, labeled and sealed. Larger samples were taken from suitable cores for organic geochemical analysis.

The working half was then sent to the Paleontology Laboratory. There, samples for shipboard and shore-based studies of nannoplankton, foraminifera, and radiolarians were taken.

The other half of a split section was designated an archive half. The cut surface was smoothed with a spatula to bring out more clearly the sedimentary features. The color, texture, structure and composition of the various lithologic units within a section were described on standard visual core description sheets (one per section), and any unusual features noted. A smear slide was made, usually at 75 centimeters if the core was uniform. Otherwise, two or more smear slides were made, each for a sediment of distinct lithology. The smear slides were examined microscopically. The archive half of the core section was then photographed. Both halves were sent to cold storage on board when they had been processed.

Some sections were not split and described on board, either because the core was too soupy and it was not believed to be representative of the sediment *in situ*, or because a large number of sections were obtained with apparently similar lithology and time was limited.

Material obtained from core catchers–and not used up in the initial examination–was retained for subsequent work in freezer boxes. Sometimes significant pebbles from the core were extracted and stored separately in labeled containers. On other occasions, the liners would contain only sediment-laden water. This was usually collected in a bucket and allowed to settle, the residue being stored in freezer boxes.

At several sites, hard cores were obtained either of basement or indurated sediment. Each separate core fragment was numbered and labeled consecutively from the top downwards, and its orientation indicated by an upward pointing arrow. Where possible the fragments were arranged into their original relative orientation and were then sliced longitudinally for examination and separation into working and archive halves.

All samples are now deposited in cold storage at the DSDP East Coast Repository at the Lamont-Doherty Geological Observatory of Columbia University, Palisades, New York. These samples may be obtained for further study.

DOWNHOLE LOGGING

It became clear during the study of the shipboard measurements of core physical properties that most major lithological changes in the cores could be inferred from the physical properties alone without lithological study. In particular, calcareous and siliceous ooze can be distinguished from terrigenous sediments, and bands of dark clay can be identified on the basis of natural gamma radioactivity. Continuous sediment density determinations showed up features such as pebbles (ice-rafted), graded beds, siliceous (opaline) sediments and even beds of foraminiferal sand within silts and clays.

Thus it is evident that a downhole logging device capable of measuring just natural gamma activity and sediment density, together with the facility for correcting these data for variations in hole diameter, will be immensely valuable. Not only will continuous data then be obtained over the uncored interval of a hole, but it might prove possible to make lithological correlations between holes on the basis of the downhole logs.

The absence of downhole logging equipment on *Glomar Challenger* during Leg 12 was therefore regretted by the shipboard scientific party, in view of the additional valuable data which could have been obtained by this means.

DRILLING CHARACTERISTICS

Since the water circulation down the hole is an open one, cuttings are lost on to the sea bed and cannot be examined. The only information available about sedimentary stratification between cores, other than from seismic data, is from an examination of the behavior of the drill string as observed on the drill platform. The harder the layer being drilled, the slower and more difficult it is to penetrate. However there are a number of other variable factors which determine the rate of penetration, so it is not possible to relate this directly with the hardness of the layers. The following parameters are recorded on the drilling recorder and all influence the rate of penetration.

(a) The weight on the bit. This can vary in three steps from zero when the bit is suspended up to 40,000 pounds when two of the three bumper subs are collapsed and the whole bottom assembly bears on the bit. The aim of the driller is to maintain constant bit weight by lowering the drill string when necessary. However, this is extremely difficult to do in conditions of swell where the heave of the drill platform may exceed the available extension (15 feet) of the bumper subs.

(b) Revolutions per minute. The revolutions per minute (r.p.m.) is related to the torque applied to the top of the drill string, and a direct analysis of the two should give the resistance to drilling. However the revolutions-per-minute record is not adequately expanded to do this. Nevertheless, visual observations of the drill rotation are useful in assessing the behavior of the bit. In particular, one can see that when the drill bit becomes jammed, rotation stops and then speeds up as it becomes free and the drill string untwists.

(c) Torque. The record of torque applied to the drill from the hydraulic drive is a more sensitive measure of the drill bit behavior and is well recorded. In Hole 111, for instance, the drill string "torqued-up" badly during the penetration of the stiff glacial clays where abundant erratic stones were found.

(d) Pump pressure and strokes per minute of water circulation. Two pumps were available to circulate water down through the drill string, past the bit and up to the sea bed in the annulus between the drill and the hole. Both pressure and rate of flow of water (in strokes per minute–s.p.m.) were recorded. Changes in circulation were one of the major factors influencing the rate of penetration. In softer sediments, more penetration was achieved by jetting the sediment out of the way rather than by cutting, so that while drilling ahead, high strokes per minute were used, whereas during coring minimum strokes were used consistent with flushing out cuttings and keeping the hole clean. Often during the cutting of a core, the holes in the bit became blocked and burst of higher circulation ("circulation breaks") were required to clear them before proceeding. These bursts of circulation were sometimes responsible for forcing soupy sediments into the core liner between harder sections. The relationship between pump pressure and rate of flow depends on the resistance to flow determined by the restrictions in the circulation path near the drill bit and in the return to the sea bed. The upward flowing water is laden with sediment cuttings and therefore exerts a net downward pressure which sometimes has to be overcome by injecting drilling muds into the circulation system. Drilling mud was also used to flush out chips of hard rocks, although only limited use of mud was possible since the circulation system was not closed.

(e) Penetration. The progress of the drill string into the bottom is recorded every 0.25 meter and every 1.0 meter on the drilling recorder; hence, penetration rates can be measured in meters per hour.

An exact interpretation of these various factors in terms of the properties of the sediments is not possible. Gross variations can be seen from the drilling records, but the more subtle changes are best assessed on the spot at the time of drilling. The driller who is constantly at the control console can assess these factors and with his long experience can make the best estimate of the nature of the bottom.

Throughout all the drilling operations one of the scientific party (A. S. Laughton, R. B. Whitmarsh or A. S. Ruffman) was on the drilling platform in close contact with the driller, the tool pusher and the drilling recorder. Notes were made on the drilling characteristics, and an interpretation of the hardness of the bottom was recorded on deck working log sheets. A graphical representation of the hardness of the bottom was developed in which the harder the strata, the heavier the shading of the appropriate section of the record. The record is reproduced in the Hole Summary charts for each site, alongside the horizons detected on the seismic reflection profiles.

In some cases, the inability to make hole was clearly the result of hard layers, such as, cherty beds, indurated sandstones, limestones or basaltic basement, as indicated by core material recovered. In other cases, however, no hard layers could be sampled and it appeared that a ball of clayey sediment had built up on the bit and spun around in the hole preventing water circulation and cushioning the bit.

DRILLING DISTURBANCES

When the cores were split many of them showed signs of the sediment having been disturbed since its deposition. Such signs were the concave downwards appearance of originally plane bands, the haphazard mixing of lumps of different lithologies and the near fluid state of some sediments recovered from tens or hundreds of meters below the sea bed (Plate 1). It seems reasonable to suppose that these disturbances came about during or after the cutting of the core. There are three different stages during which the core may suffer stresses sufficient to alter its physical characteristics from those of the *in situ* state. These stages are the cutting, retrieval (with accompanying changes in pressure and temperature), and handling of the core.

During drilling six basic parameters (bit type, weight on the bit, pipe revolutions per minute, torque, pump pressure and pump strokes per minute) reflect the conditions at the contact between bit and sediment. When a core is being cut water circulation is reduced to a minumum, or zero, and bit weight is normally kept to lower values and increased more steadily than during drilling. Invariably however some short periods of circulation are required and it is then that softer sediments may be washed away from the bit or that water may be forced up inside the core liner turning the sediment to a slurry. The washing away of softer sediment during periods of circulation can lead to the recovered cores being unrepresentative samples of the drilled strata. This is especially so when alternating hard and soft beds are being cut, as happened at Sites 111, 115, 116 and 118. The heave of the bit while coring during rough weather may also lead to fluid cores and this may have been the reason for retrieving such cores at Sites 114 and 116.

Due to the relatively large compressibility and thermal expansion of water, the sea-water in cores can experience volume changes of several per cent during the recovery of the core. The stresses imposed on cores by the varying combinations of changes of temperature, hydrostatic pressure and overburden pressure cannot be calculated precisely. Hydrostatic pressure will decrease linearly with decreasing depth while the core temperature at any depth will depend on the temperature generated during coring, the geothermal gradient, and the depth and temperature of the sea. In cases of high porosity sediments the sea-water volume changes may be accommodated by free flow between mineral grains, however in lower porosity sediments the grain framework may prevent sufficiently rapid egress of water and in these cases the sediment framework may burst apart and be reduced to a slurry. This explanation is put forward for the almost fluid cores sometimes recovered, especially for the watery patches in cores which are otherwise coherent, although it is realized that some watery cores may reflect the effect of unfavorable drilling parameters during coring as discussed above. Some cores degassed in the laboratory and this may also have caused the breakdown of the grain framework in some cases.

Usually the net effect of the above two sets of stresses will be to alter the mechanical properties of the sediment. Richards (for example, 1962) has studied many aspects of core disturbance on such properties and has found that shear strength is invariably reduced by the coring process. Some sediments, especially those rich in clay minerals, may behave thixotropically but the rate at which the sediment strength returns is unknown and may be slower than the experimenter can afford to wait. The effect of the coring process on the elastic moduli, and hence on the compressional wave velocity of the sediment is unknown.

The deformation which occurs during core handling is mostly confined to transverse breaks in the cores caused by flexing the plastic liners or by the splitting process.

On the basis of the visual core descriptions four classes of disturbed core were set up, defined as follows:

Class 1, those parts of cores described as void, empty or partly filled.

Class 2, those parts of cores described as watery, sloppy, or soupy (Plate 1C), or with a type of disturbance where two lithologies have become mixed, the harder lithology forming lumps in a soft wet matrix of the second one, or when the core has been described as disrupted, as a drilling breccia or as A in a matrix of B (Plate 1D); also all those watery sections which were not split, other unsplit sections are also included for convenience.

Class 3, those parts of cores described as disturbed, flow disturbed, flow in or plastic. Such cores are characterized by obvious plastic deformation of the sediment (Plate 1B).

Class 4, those parts of cores not described by terms suggesting deformation. Usually such cores are indurated and have transverse breaks (Plate 1A), but they can be softer uniform lithologies in which deformation may have occurred but because of the uniform lithology there is no visible evidence of it.

All the cores were subdivided into the above four classes of disturbance according to their visual core descriptions. On the basis of such disturbance logs it was initially intended to omit from the Core and Hole Summaries physical property measurements over parts of cores assigned to classes 1 and 2. However on inspecting the GRAPE data incompatabilities with the disturbance log were found due to the core having slipped inside the liner between the time the GRAPE measurement was made and the time the visual core description was formulated after the core had been split. In these cases, the disturbance log was edited accordingly to give the original arrangement of void spaces to aid the data processing of large numbers of GRAPE and natural gamma measurements. (It should be noted however that because of this editing it becomes possible for measurements made after the core was split—penetrometer, grain size, carbonate and water content—to appear on the summary forms to originate from void segments of core, but the reader may allow for this by mentally rearranging the core.) In other cases the visual core description was shown to be inconsistent or deficient in the description of the degree of disturbance as judged by the GRAPE values. Therefore it was decided to plot on the summary forms all the physical properties measured on cores of classes 2, 3 and 4 and to leave the judgement of the quality of the data to the reader.

A different type of disturbance was noticeable at Sites 119 and 117 where anomalously young microfossils were found in some cores. At Site 119, Miocene radiolarians were found in the core catchers of cores of Oligocene to Eocene age; and, at Site 117 Miocene coccoliths were found in cores of late Oligocene age and older. This type of anomaly is attributed to picking up material which has fallen down the hole during drilling probably due to the reduced water circulation during coring and core barrel operations. This paleontological problem is discussed in detail in the relevant site chapters.

BASIS FOR AGE DETERMINATION

General

A Cretaceous time-scale (van Hinte, 1971) is shown in Figure 2 and a Cenozoic one (Berggren, 1971) in Figure 3. These form the basis for age determinations of biostratigraphic or time-stratigraphic levels encountered on Leg 12. Various systems of zonation based upon calcareous plankton exist for the Mesozoic and Cenozoic. Since the completion of our cruise the radiolarian zonation for the Cenozoic (post Early Eocene) has appeared, and it has been possible to integrate this zonation with a standard scheme for the calcareous plankton (Figure 4-6).

Foraminifera

Mesozoic (J.E.vH.)

The Mesozoic age determinations are primarily based on the occurrences of particular, diagnostic, planktonic foraminifers. But in part of the section planktonic foraminifers were absent or their evidence was inconclusive and we had to rely upon benthonic foraminifers and ostracods. Fortunately the material allowed for direct comparison with Western European faunas and with stratotypes of stages (see Mesozoic section of Site 111).

Cenozoic (W.A.B.)

Cenozoic age determinations were based primarily upon planktonic foraminiferal assemblages. The standard system of zonation used is that by Blow (1969) for the post Middle Eocene and one devised by Blow and Berggren and since modified slightly by Berggren (1971) for the Paleocene-Middle Eocene (Figures 3, 4). If Leg 12 proved anything, it was that a system of zonation based essentially upon tropical (low-latitude) forms is not applicable to the Cenozoic sediments of the North Atlantic. As a result an attempt was made to determine ages in terms of equivalency to a particular planktonic foraminiferal zone wherever possible. Where this was not possible, age determinations in terms of a particular epoch/series subdivision (for example, Early Miocene) were made.

On the basis of the Cenozoic foraminiferal faunas encountered in the northern part of the North Atlantic (Sites 111 through 117), a multiple system of zonation has been devised which can, in turn, be correlated broadly with

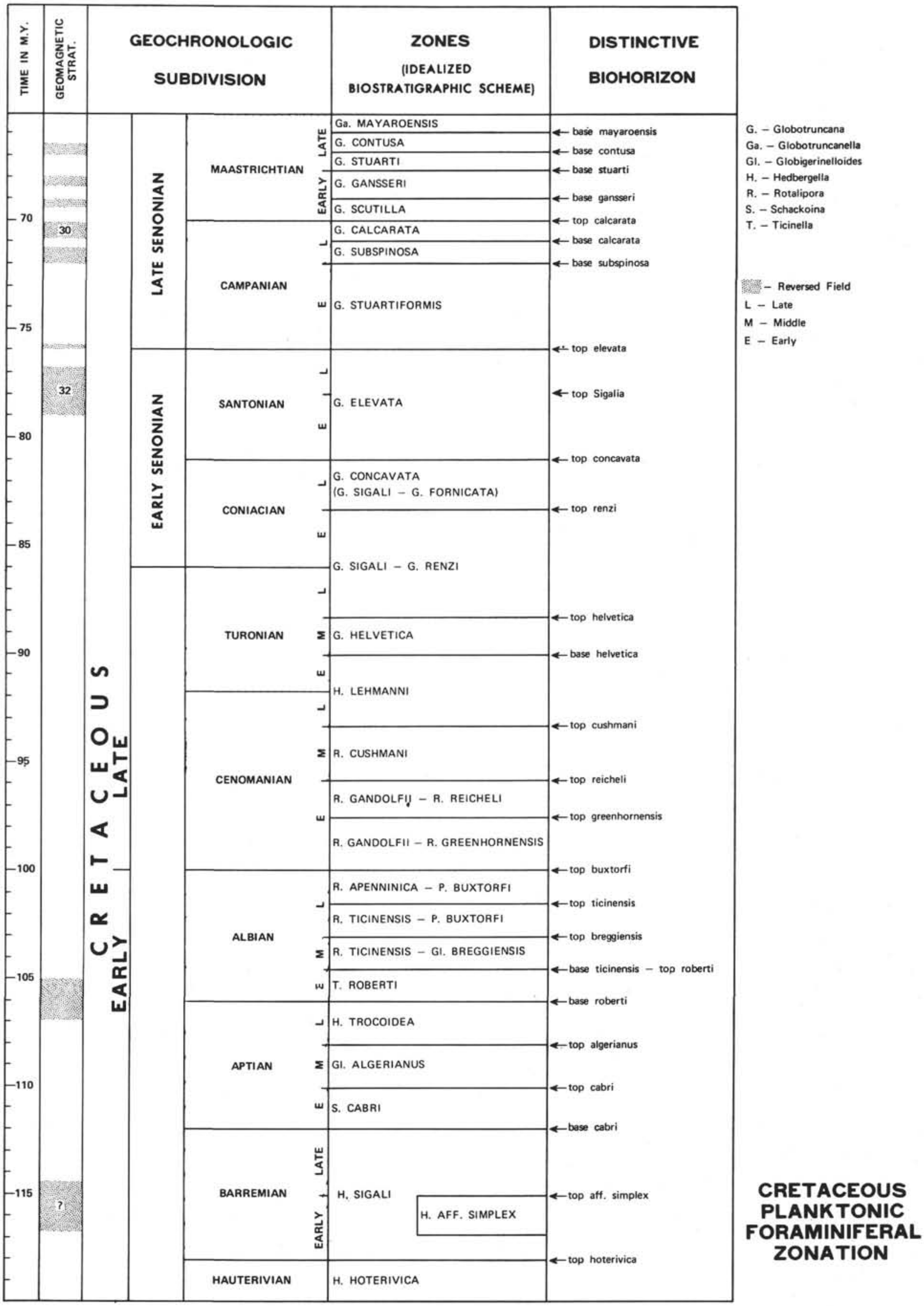

Figure 2. *Cretaceous planktonic foraminiferal zonation.*

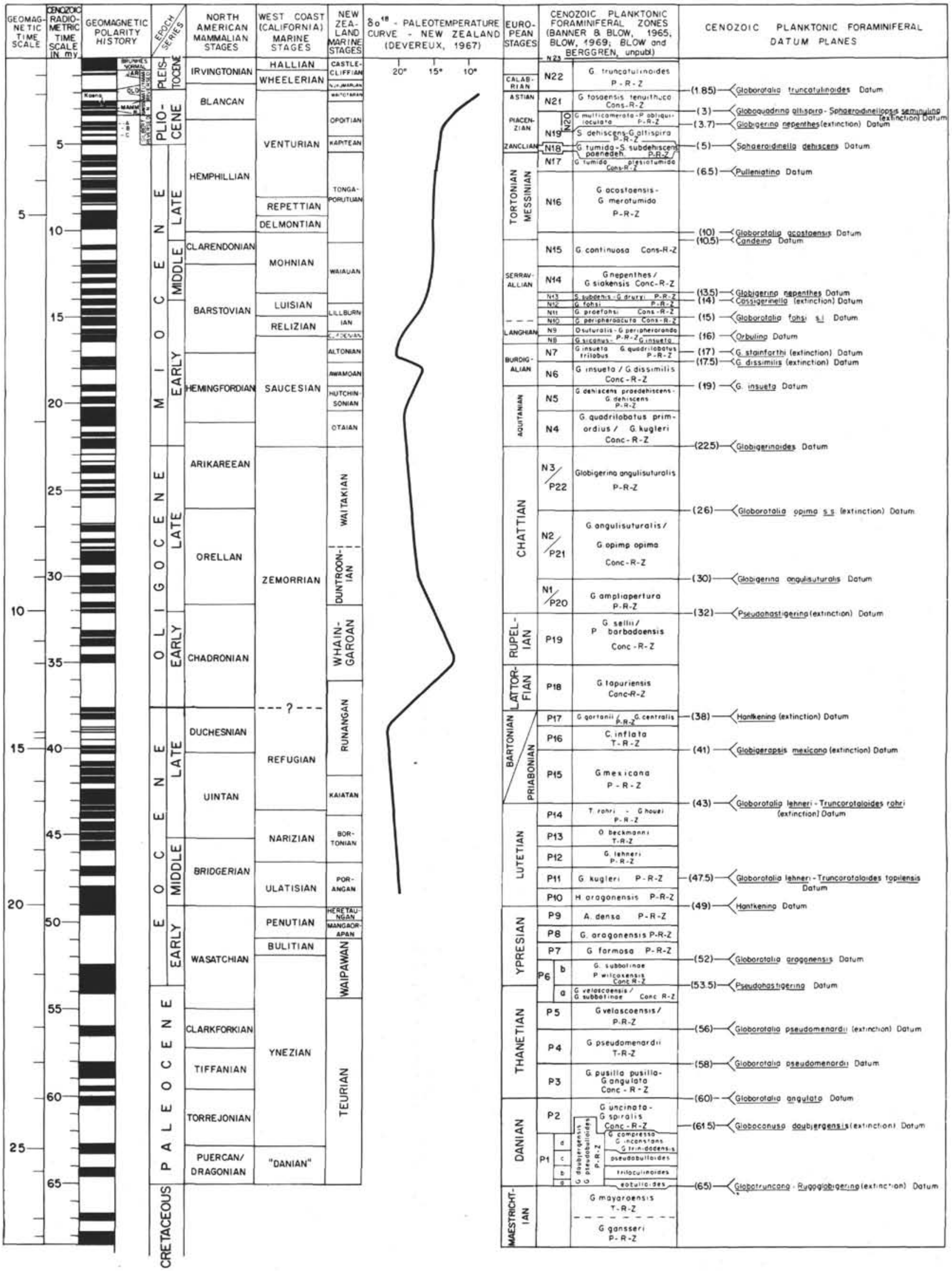

Figure 3. *Tertiary planktonic foraminiferal zonation.*

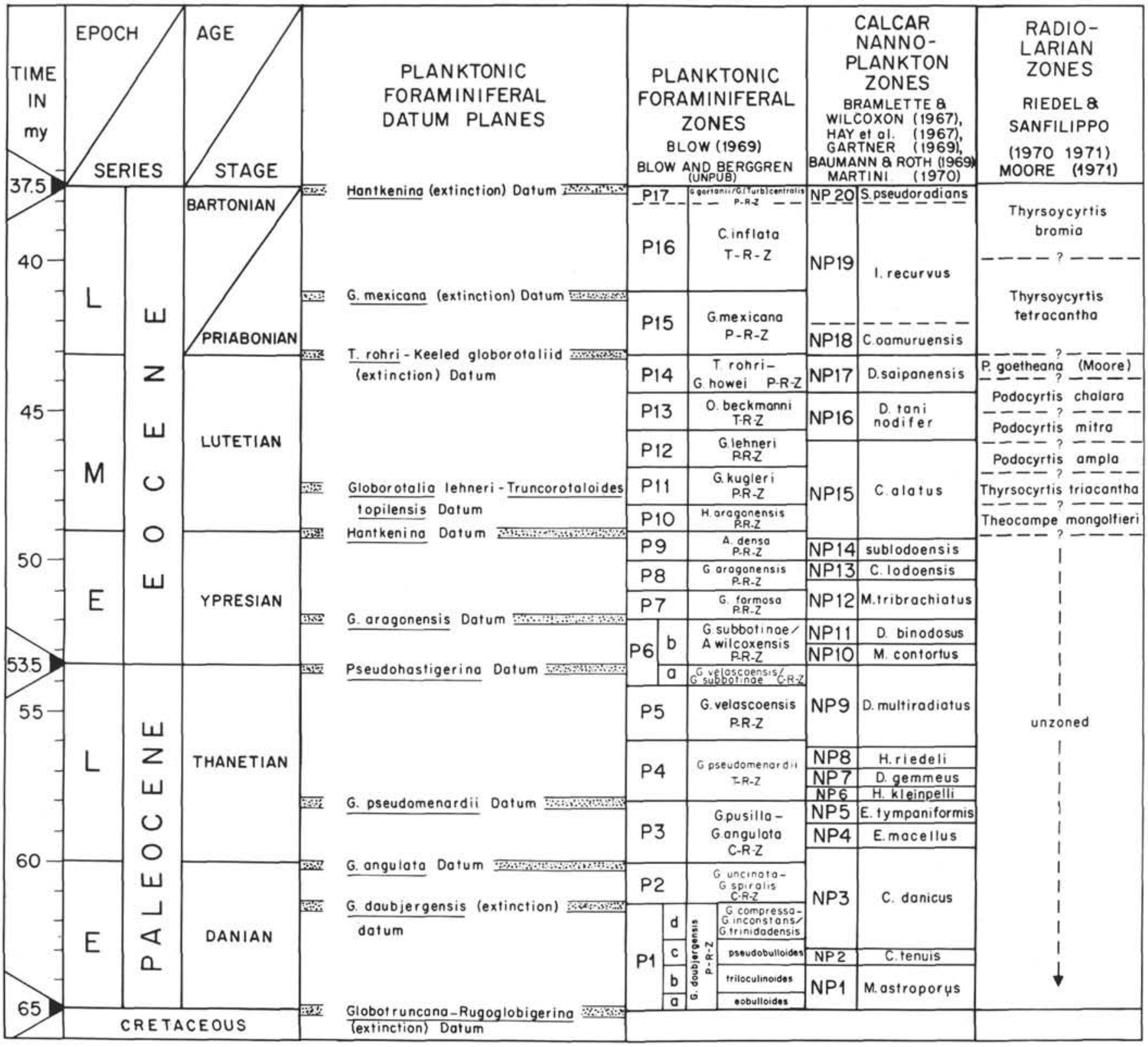

Figure 4. *Correlation of foraminiferal, radiolarian and nannofossil zones for the Eocene and Paleocene.*

the tropical zonation scheme. This is discussed more fully in the secton on Paleobiogeography and Biostratigraphy of the North Atlantic (Chapter 14). This multiple zonation is based upon associations of species, is biostratigraphic in nature, and is not formally defined. In general, it was found easier to apply the existing tropical (low-latitude) zonation scheme in the North Atlantic in the Paleogene than in the Neogene (this is also true for calcareous nannoplankton; see below). This is due to the gradual latitudinal provincialization of planktonic faunas during the Cenozoic, discussed in greater detail in Chapter 14.

Calcareous Nannofossils (K.P.N.)

The coccolith zones used in this report follow mainly the "standard calcareous nannoplankton zonation" proposed by Martini (1970) for the Paleogenc and by Martini and Worsley (1970) for the Neogene. The modifications made include the use of the "*Coccolithus jaramillensis*" Zone in the Pleistocene and the *Discoaster neohamatus* Zone instead of the *Discoaster calcaris* Zone in the Miocene. At the Oligocene-Miocene boundary, the *Discoaster druggi* Zone and the *Triquetrorhabdulus carinatus* Zone could not be distinguished. In the Lower Oligocene, the *Ericsonia? subdisticha* Zone is replaced by the *Ericsonia obruta* Zone. In the Eocene, the *Chiasmolithus oamaruensis* Zone is changed to *Reticulofenestra umbilica* Zone and *Chiphragmalithus alatus* to *Nannotetrina fulgens* (for systematical reasons). The Paleocene *Heliolithus riedeli* Zone is replaced by the *Discoaster nobilis* Zone. In the Maestrichtian, three zones were recognized: the *Tetralithus*

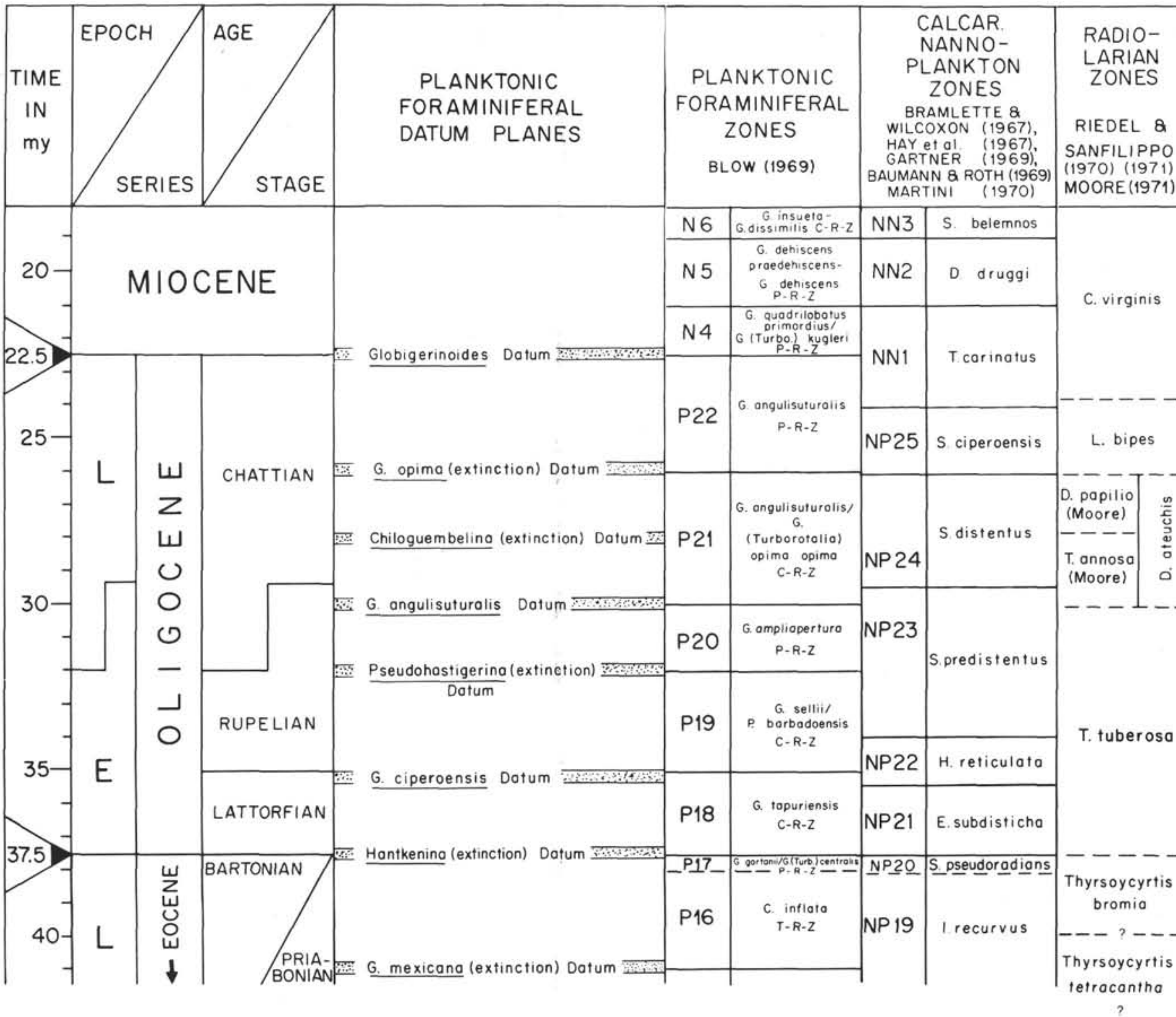

Figure 5. *Correlation of foraminiferal, radiolarian and nannofossil zones for the Oligocene and Lower Miocene.*

murus-Nephrolithus frequens Zone at the top, the *Arkhangelskiella cymbiformis* and *Reinhardtites anthophorus* Zone below. No attempt was made to assign the Albian and Cenomanian deposits recovered at Site 111 to calcareous nannofossil zones.

For the definitions used for the zones in this report and the check-list of species utilized, see Chapter 15.

Radiolaria (R.N.B.)

The radiolarian zonation utilized in this report is based upon those recently proposed by Riedel and Sanfilippo (1970, 1971) and Moore (1971).

LITHOLOGICAL NOMENCLATURE AND SYMBOLS

At the present time there seems to be no universally applicable descriptive classification of deep sea sediments. Many of the classification schemes which have been proposed suffer from the limitation that they consider only one characteristic of the sediments, for example, carbonate content, texture, etc. Other schemes are too subjective in the sense that they demand a genetic interpretation of the sediment before a descriptive name can be assigned. While some interpretation may be inevitable and a close correspondence between descriptive classification and mode of origin is certainly desirable (Pettijohn, 1957) it is a moot point to what extent interpretation should precede classification and description. The scheme proposed by Olausson (1960) and advised by the JOIDES Panel on Sedimentary Petrology, for example, is in our view impractical since it demands that the observer decide in advance whether a sediment is terrigenous or pelagic. It is our observation that in the North Atlantic region the processes of sedimentation operating are sufficiently complex that this simple division

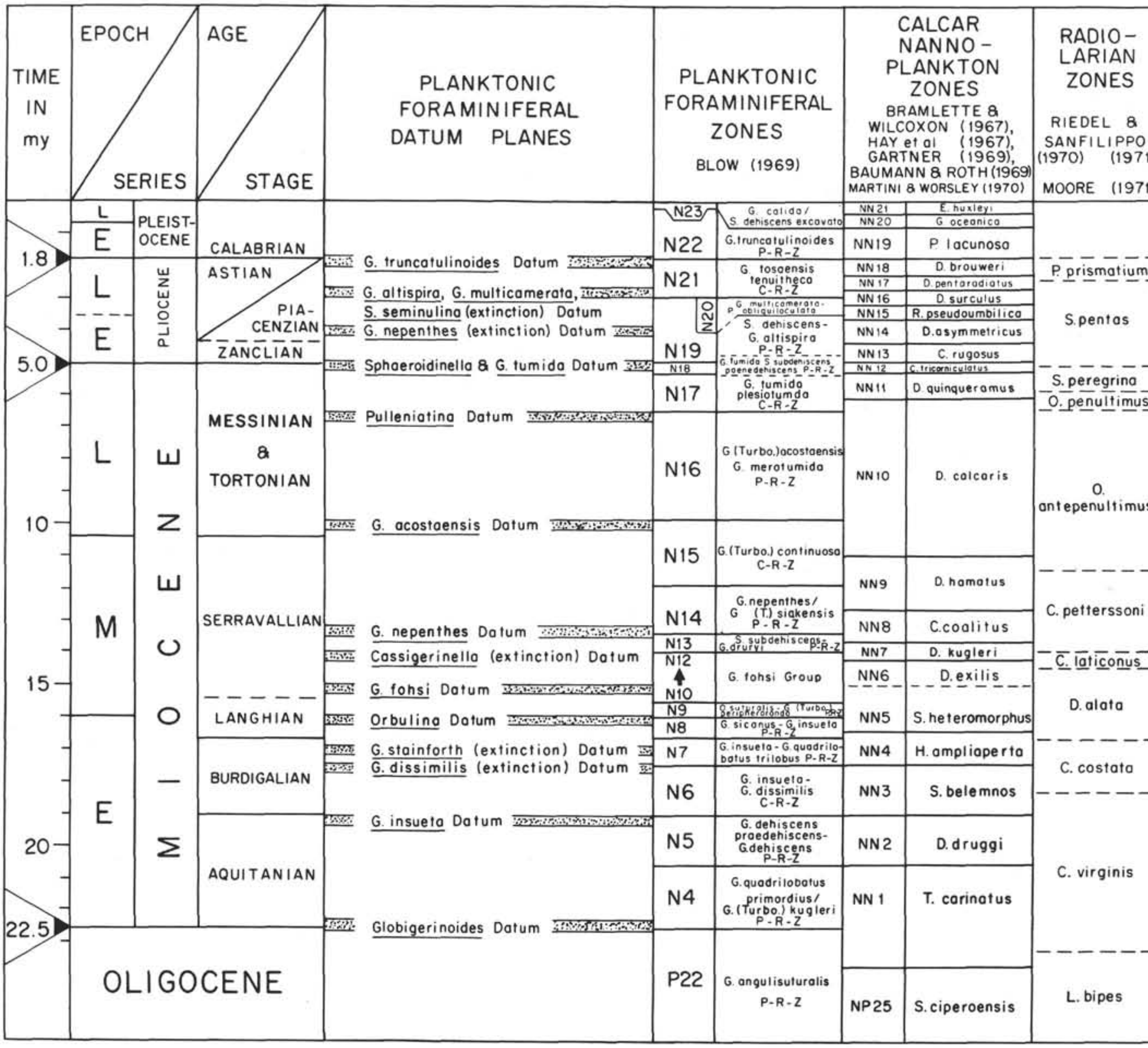

Figure 6. *Correlation of foraminiferal, radiolarian and nannofossil zones for the Miocene, Pliocene and Pleistocene.*

into two broad classes of sediment cannot be considered realistic, and the scheme thus breaks down.

The scheme we have used is illustrated in Figure 7. Rather than devising yet another neat and tidy textbook classification and then attempting to fit the sediments into it we have adopted the opposite approach and tried to use a fairly objective terminology developed from the sediments themselves, leaving the way clear for any subsequent discussion of origins and mechanisms of formation. Since the scheme grew along with our experience there is, inevitably, a certain amount of unevenness in usage. The terms "claystone," "indurated clay" and "lithified" or "semi-lithified clay," for example, have been used more or less interchangeably. Also it should be pointed out that we have used the term "chalk," not in the sense of Olausson (1960) to imply only carbonate content, but in its original and more widely understood sense to mean a soft friable rock which is almost entirely carbonate (Pettijohn, 1957). Similarly it should be noted that the term "marl" is used with its broader meaning of simply a calcareous clay and not with the restricted meaning applied by Olausson (1960).

We do not pretend that the scheme used here is perfect or universally applicable, or even logically defensible. However, we did find it to be easily applied and understood. We believe that the reader will find that it does fulfill one of the main purposes of a descriptive classification: that of facilitating communication.

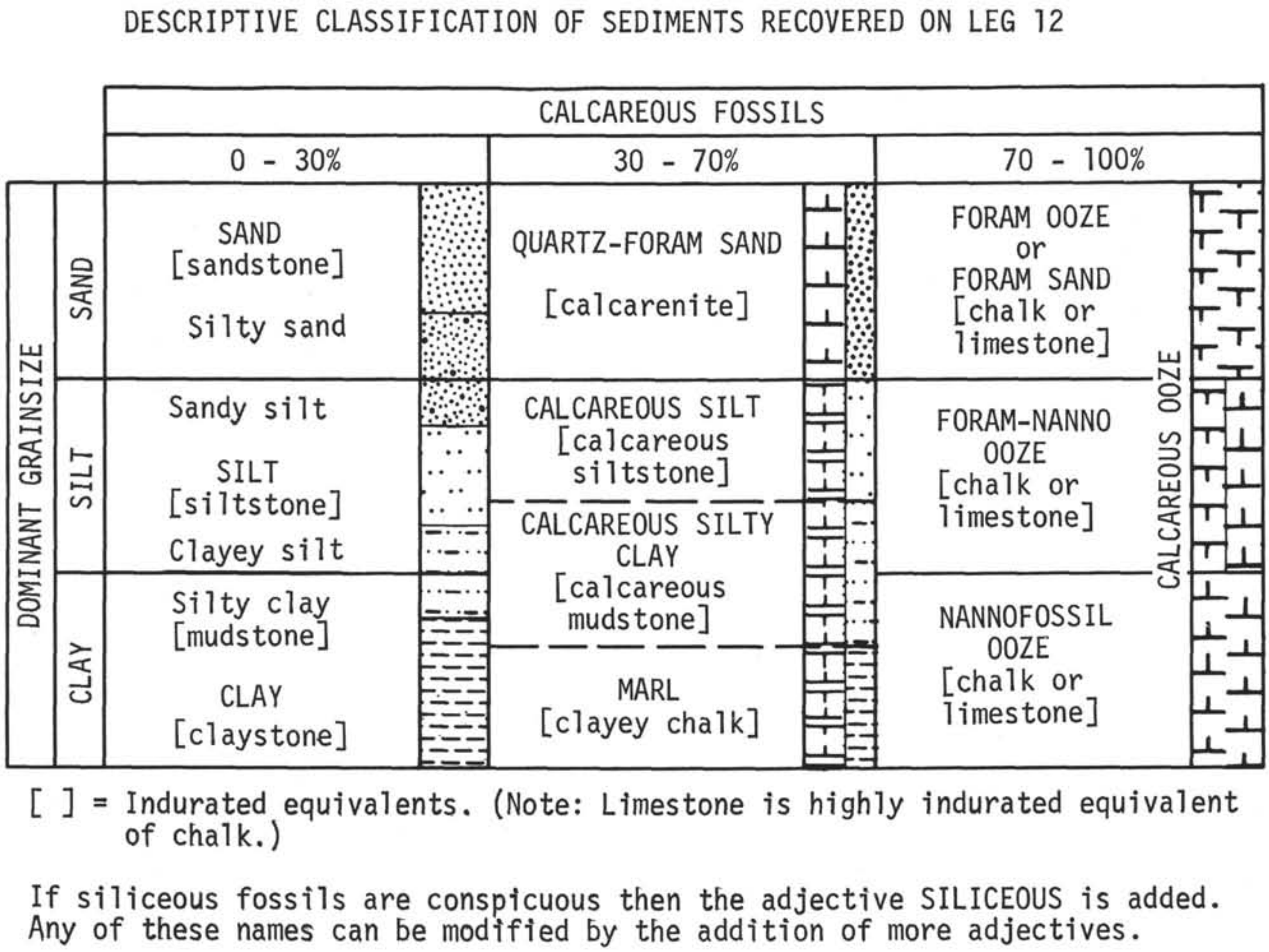

Figure 7. *Descriptive classification of sediments recovered on Leg 12.*

GRAIN SIZE ANALYSES

Grain size distribution was determined by standard sieving and pipette analysis. The sediment sample was dried, then dispersed in a calgon solution. If the sediment failed to disaggregate in calgon, it was dispersed in hydrogen peroxide. The sand-sized fraction was separated by a 62.5-micron sieve with the fines being processed by standard pipette analysis following Stokes settling velocity equation (Krumbein and Pettijohn, 1938, p. 95-96) which is discussed in detail in Volume IX of the *Initial Reports of the Deep Sea Drilling Project.* Step-by-step procedures are in Volume V. In general the sand-, silt-, and clay-sized fractions are reproducible within ±2.5 per cent (absolute) with multiple operators over a long period of time. A discussion of this precision is in Volume IX.

CARBON AND CARBONATE ANALYSES

The carbon-carbonate data were determined by an Leco induction furnace combined with a Leco acid-base semiautomatic carbon determinator. Normally, the more precise seventy-second analyzer is used in place of the semiautomatic carbon determinator, but it was not used for these samples because it was undergoing modifications.

The sample was burned at 1600°C and the liberated gas of carbon dioxide and oxygen volumetrically measured in a solution of dilute sulfuric acid and methyl red. This gas was then passed through potassium hydroxide solution, which preferentially absorbs carbon dioxide, and the volume of the gas was measured a second time. The volume of carbon dioxide gas is the difference of the two volumetric measurements. Corrections are made to standard temperature and pressure. Step-by-step procedures are in Volume IV of the *Initial Reports of the Deep Sea Drilling Project* and a discussion of the method, calibration, and precision are in Volume IX.

Total carbon and organic carbon (carbon remaining after treatment with hydrochloric acid) are determined in terms of percent by weight, and the theoretical percentage of calcium carbonate is calculated from the following relationship:

$$\text{Per cent calcium carbonate } (CaCO_3) = (\%\text{ total C} - \%\text{ C after acidification}) \times 8.33$$

However, carbonate sediments may also include magnesium, iron, or other carbonates; this may result in "calcium" carbonate values greater than the actual content of calcium carbonate. In our determinations, all carbonate is assumed to be calcium carbonate.

Precision of the determination is as follows:

Total carbon (within 1.2 to 12%)	= ± 0.3% absolute
(within 0 to 1.2%)	= ± 0.06% absolute
Organic carbon	= ± 0.06% absolute
Calcium carbonate (within 10-100%)	= ± 3.0% absolute
(within 0-10%)	= ± 1.0% absolute

X-RAY METHODS

Samples of sediment were examined using X-ray diffraction methods at the University of California at Riverside, under the supervision of R. W. Rex and H. E. Cook.

Treatment of the raw samples was: washing to remove seawater salts, grinding to less than 10 microns under butanol, and expansion of montmorillonite with trihexylamine acetate. The sediments were X-rayed as randomized powders. A more complete account of the methods used at Riverside is found in Chapter 19 of this volume.

The data are tabulated in Chapter 19. Columns one and two contain the core numbers and the depths of the cored intervals (in meters below the mudline). The third column gives the depths of the composited, sample intervals or the depths of single samples. Column 4 contains the percentage of the diffuse scattered X-rays to the Bragg and diffuse scattered X-rays. The amorphous scattering percentage in column 5 is derived from the data of column 4 by a simple conversion based on the ratio of Bragg and diffuse scattering in pure quartz. It is a measure of the proportion of crystalline and amorphous materials in the sample. The remaining columns contain crystalline mineral percentages computed by the method of mutual standards using peak heights.

PHYSICAL PROPERTIES

Natural gamma radioactivity

Barsukov *et al.* (1964) mention the natural occurrence of 40 radioactive elements and 16 of these elements, comprising 42 isotopes, emit gamma rays (Lederer *et al.*, 1967). The majority of gamma rays emitted from sedimentary rocks come from the radioactive isotopes forming the three natural decay series of uranium, protactinium (from U^{235} parent) and thorium and from potassium-40 (Table 1). Except for U^{234}, Th^{230} and Pa^{231}, the daughter isotopes of the decay series all have half-lives which are geologically insignificantly small. For pre-Quaternary cores, a radioactive equilibrium will have been reached in each series so that the concentrations of daughter isotopes will be determined by the amount of the corresponding parent isotope (U^{238}, U^{235}, or Th^{232}) in the sediment. The remaining naturally gamma-emitting isotopes (these are Al^{26}, V^{50}, Te^{123}, La^{138}, Lu^{176}) have such long half-lives and/or small percentage isotopic abundances that even element concentrations of 10 ppm in the sediment would not appreciably affect the gamma-ray count. Some gamma-ray emitting radionuclides with geologically significant half-lives are produced by the action of cosmic rays on the atmosphere and of solar protons on interplanetary dust, but only insignificant quantities of such isotopes occur in marine sediments (Amin *et al.*, 1966; Wasson, 1963).

The primary sources of uranium and thorium are igneous rocks. These rocks are broken down on the continents by weathering and the radioactive elements are carried into the sea within rock particles or in solution. On the sea floor the uranium and thorium may accumulate by adsorption onto clays. Adams (1962) states that at least two-thirds of the uranium and thorium in the lithosphere is contained in fine-grained (circa tens of microns) accessory minerals, such as zircon and monazite, which may be included in biotite. Uranium is also taken up during the formation of marine carbonates such as oolites and corals, reaching a concentration of about 3 ppm, but in foraminifera, molluscs and echinoids the concentration is about 100-fold less (Prospero and Koczy, 1966; Broecker, 1963; Tatsumoto and Goldberg, 1959). Potassium-40 makes up 0.0119 per cent of naturally occurring potassium. There is no evidence of any significant development of authigenic minerals containing potassium in marine sediments, hence all the potassium is of detrital origin (Prospero and Koczy, 1967). Significant gamma counts due to potassium-40 depend on the presence of potassium-rich minerals such as, glauconite (7.6 per cent potassium by weight), orthoclase feldspar (14.0 per cent), micas (muscovite 9.8 per cent, biotite 9.4 per cent), leucite (17.9 per cent) and some zeolites (phillipsite 8.2 per cent), plus evaporite products such as nitre (38.6 per cent), sylvine (52.4 per cent), etc. Clay minerals are selectively efficient in "fixing" potassium (Adams, 1962).

Barsukov *et al.* (1964) indicate that the radioactivity of sedimentary rocks increases with the following factors:

(1) Increasing argillaceous material, due to uranium and thorium adsorption by such matter.

(2) Slow rates of accumulation, during which the amount of uranium precipitated from solution increases.

(3) Increasing content of potassium-rich minerals.

(4) A transition from reddish to gray and black shales since dark rocks indicate a reducing environment where hexavalent uranium alters to less soluble tetravalent uranium which is precipitated. Dark rock also indicates more organic matter of colloids, which adsorb uranium and thorium ions.

(5) Decreasing porosity, because there is more rock per unit volume.

Detailed descriptions of the natural gamma counting equipment used on board *Glomar Challenger* are given by Evans and Lucia (1970). One-thousand counts per nominal 7.6 centimeters[1] of core per 75 seconds, as measured by the gamma-ray counter on board *Glomar Challenger*, are approximately equivalent to 1600 disintegrations per minute (dpm)/kg of dry sediment, assuming the sediment porosity is 60 per cent. From adding the activities of K^{40} and the three natural decay series (column 6, Table 1) it is apparent that a core of Recent sea-bed sediment should give a count of at least 9700 in contrast to the normally observed shipboard value of several hundred counts for

[1]The length which is effectively scanned in greater than 7.6 cm and is assumed for this calculation to be 10 cm.

TABLE 1

Decay Step (1)	Half-life (2)	γ-ray Energy (Mev) (3)	γ-ray Intensity (%) (4)	Abundance in Young Marine Sediment (g/kg) (5)	γ-rays Emitted by Young Sediment (dpm/kg) (6)	γ-rays Emitted by Older Sediment (dpm/kg) (7)
Uranium Series						
$U^{238} \rightarrow Th^{234}$	4.51×10^{9}y	0.048	23.00	1×10^{-3} $(0.4\text{-}80) \times 10^{-3}$	12	12
$Th^{234} \rightarrow Pa^{234}$	24.1d	0.029-0.092	7.5	1.4×10^{-14}	39	39
$Pa^{234} \rightarrow U^{234}$	1.18m	0.765,1.001	1.00	4.7×10^{-17}	517	517
$U^{234} \rightarrow Th^{230}$	2.48×10^{5}y	0.053	0.20	8.1×10^{-8} $(2.4\text{-}490)10^{-8}$	2	2
$Th^{230} \rightarrow Ra^{226}$	75,200y	0.068	0.72	2×10^{-7} $(1\text{-}30) \times 10^{-7}$	48	4
$Ra^{226} \rightarrow Rn^{222}$	1620y	0.186	4.00	4×10^{-9} $(0.3\text{-}40) \times 10^{-9}$	250	21
$Rn^{222} \rightarrow Po^{218}$	3.823d	0.510	0.07	2.5×10^{-14}	4	0
$Po^{218} \rightarrow Pb^{214}$	3.05m	–	–	1.4×10^{-17}	–	–
$Pb^{214} \rightarrow Bi^{214}$	26.8m	0.242-0.352	60.00	1.2×10^{-16}	3808	317
$Bi^{214} \rightarrow Po^{214}$	19.7m	0.609-2.445	119.00	8.8×10^{-7}	7543	628
$Po^{214} \rightarrow Pb^{210}$	1s	0.800	0.00	1.1×10^{-24}	–	–
$Pb^{210} \rightarrow Bi^{210}$	22y	0.047	4.00	4.5×10^{-11}	257	21
$Bi^{210} \rightarrow Po^{210}$	5d	–	–	3.1×10^{-14}	–	–
$Po^{210} \rightarrow Pb^{206}$	138.4d	0.800	0.00	8.8×10^{-13}	0	0
					12480	1561
Protactinium Series						
$U^{235} \rightarrow Th^{231}$	7.13×10^{8}y	0.110-0.204	79.00	7.1×10^{-6} $(2.8\text{-}580) \times 10^{-6}$	19	19
$Th^{231} \rightarrow Pa^{231}$	25.6h	0.026,0.084	26.00	2.9×10^{-17}	6	6
$Pa^{231} \rightarrow Ac^{227}$	32480y	0.027,0.290	12.00	1×10^{-8} $(0.5\text{-}15) \times 10^{-8}$	92	92
$Ac^{227} \xrightarrow{98.8\%} Th^{227}$	21.2y	0.009-0.025	weak	5.9×10^{-12}	0	0
Th^{227} Ra^{223}	18.17d	0.050-0.310	31.00	1.3×10^{-14}	206	7
$Ra^{223} \rightarrow Rn^{219}$	11.7d	0.149-0.330	26.00	8.5×10^{-15}	172	6
$Rn^{219} \rightarrow Po^{215}$	4s	0.272,0.401	14.00	3.1×10^{-20}	89	3
$Po^{215} \rightarrow Pb^{211}$	1s	–	–	1.4×10^{-23}	–	–
$Pb^{211} \rightarrow Bi^{211}$	36.1m	0.405-0.832	9.60	1.6×10^{-17}	58	2
$Bi^{211} \xrightarrow{99.7\%} T1^{207}$	2.15m	0.350	14.00	1×10^{-18}	101	3
$T1^{207} \rightarrow Pb^{207}$	4.78m	0.897	0.16	2.1×10^{-18}	1	0
					744	138

TABLE 1 – *Continued*

Decay step (1)	Half-life (2)	γ-ray Energy (Mev) (3)	γ-ray Intensity (%) (4)	Abundance in Young Marine Sediment (g/kg) (5)	γ-rays Emitted by Young Sediment (dpm/kg) (6)	γ-rays Emitted by Older Sediment (dpm/kg) (7)
Thorium Series						
$Th^{232} \rightarrow Ra^{228}$	1.41×10^{10}y	0.059	24.00	5×10^{-3} $(2\text{-}12) \times 10^{-3}$	211	211
$Ra^{228} \rightarrow Ac^{228}$	5.7y	very weak	–	2.3×10^{-12}	0	0
$Ac^{228} \rightarrow Th^{228}$	6.13h	0.340-0.965	60.00	2.4×10^{-16}	528	528
$Th^{228} \rightarrow Ra^{224}$	1.91y	0.085-0.214	2.25	7×10^{-13}	21	21
$Ra^{224} \rightarrow Rn^{220}$	3.64d	0.241	3.70	3.4×10^{-15}	30	30
$Rn^{220} \rightarrow Po^{216}$	56s	0.550	0.07	5.4×10^{-19}	0	0
$Po^{216} \rightarrow Pb^{212}$	1s	–	–	1.7×10^{-21}	–	–
$Pb^{212} \rightarrow Bi^{212}$	10.64h	0.239,0.300	50.00	3.9×10^{-16}	421	421
$Bi^{212} \xrightarrow{66.3\%} Po^{212}$	60.6m	0.727,1.620	11.50	3.7×10^{-21}	98	98
$Bi^{212} \xrightarrow{33.7\%} Tl^{208}$	60.6m	0.040	2.00		17	17
$Po^{212} \rightarrow Pb^{208}$	1s	–	–	2.4×10^{-26}	–	–
$Tl^{208} \rightarrow Pb^{208}$	3.1m	0.511-2.614	221.00	6.7×10^{-19}	707	707
					2033	2033
K^{40} A^{40}	1.25×10^{9}y	1.460	11.00	$(0.44\text{-}11.9) \times 10^{-3}$ $(0.8\text{-}4.5) \times 10^{-3}$	770-19,800	770-19,800

Columns (1) and (2), naturally radioactive decay series and their half-lives taken from Prospero and Koczy (1967). In column (2) y = years, d = days, h = hours, m = minutes, s = seconds.

Column (3), the gamma-ray energies quoted are the most important ones to the range which they cover if there are several, from Lederer *et al.* (1967). Dashes indicate that no gamma rays are emitted.

Column (4), gamma-ray intensities from Lederer *et al.* (1967).

Column (5) contains average (Koczy and Rosholt, 1962), and observed (Koczy and Rosholt, 1962; Prospero and Koczy, 1967) ranges of abundances per kilogram of dry sediment. Most of the average concentrations are the expected values in equilibrium with the few isotopic concentrations which have been measured directly, i.e. those of uranium, thorium, protactinium, radium.

Column (6) is derived from the half-life, average abundance and gamma-ray intensity of each radioactive isotope in the series, using the formula:

$$\text{rate of emission} = \frac{\text{abundance} \times \text{atomic wt. of } H_2 \times \gamma - \text{ray intensity}}{2 \times \text{mass number} \times \text{half-life} \times \text{mass hydrogen atom}}$$

1600 dpm/Kg are approximately equivalent to 1000 counts/7.6 cm of 60% porosity core/75 secs. as measured on *Glomar Challenger.*

Column (7) is derived from column (6) and represents the counts expected after all non-uranium supported quantities of Th^{230} and Th^{227} have decayed away (about 2.6×10^{5}y) and before the amounts of the parent isotopes have appreciably decreased (several hundred million years).

oozes and clays. There are several reasons for this discrepancy. (1) The sediment may be much poorer in uranium and thorium than the average abundances in Table 1 but the quoted ranges of values indicate a maximum possible reduction of the expected count rate by a factor of only 2.5. It has been pointed out however that the average Th^{232} concentration (thorium series) is that of an especially thorium-rich Central Pacific red clay and lower values are found in the Atlantic (Picciotto and Wilgain, 1954). (2) The total count from the uranium series is increased by the initial concentration of non-uranium supported Th^{230}. This isotope will have reached an equilibrium concentration with U^{238} after about 2.6×10^{5} years, so that the contributions of this isotope and succeeding ones in the series will decrease 12-fold giving a minimum total of 980 counts for this series. The contribution from the protactinium series will also be much reduced after about 1.6×10^{5} years when the initial non-uranium supported Pa^{231} has decayed to form an equilibrium series with the parent isotope, and the activity of this and succeeding members of the series will have decreased about 30-fold giving a total of 86 counts. (3) The crystals of scintillation counters respond less to low energy gamma-rays because of the energy required to penetrate the crystals. Preliminary results of tests by C. Collier (personal communication) on the natural-gamma equipment on *Glomar Challenger* indicate that the counter sensitivity decreases tenfold for gamma-rays of 0.15 MeV and less. In actual fact this effect will barely reduce the counts in column 7 of Table 1 for the uranium series, will make the protactinium series even less significant, and will decrease the counts from the thorium series by about 10 per cent.

Clearly for cores older than about 2.6×10^5 years, and younger than several hundred million years, important contributions to natural gamma activity come from the uranium and thorium series and from potassium-40 (column 7, Table 1). The protactinium series appears to be unimportant in such cores. Any counts in excess of 2350 will be due to K^{40} decay alone, or else to a greater concentration of U^{238} and/or Th^{232} than the average values in Table 1.

It is interesting to note that the rate of decay of gamma activity with depth in sediments less than 2.6×10^5 years old can be used to calculate an estimate of the mean rate of sedimentation provided the lithology and sedimentation rate are fairly constant.

The natural gamma counts plotted in this volume were derived by subtracting from the observed counts the mean value of the background radiation measured with air and water standards inserted in the counter, and then correcting to the counts expected if each core had a porosity of 60 per cent by multiplying by the factor 40/(100-% porosity). As mentioned above natural gamma activity is dependent on porosity, but since this parameter has been independently measured by the GRAPE (gamma-ray attenuation porosity evaluator) its effect on the gamma count can be removed. This procedure is believed to be justified because the concentrations of the radioactive parent isotopes and K^{40} in sea-water are at least an order of magnitude less than the minimum concentrations found in deep-sea sediments (Koczy and Rosholt, 1962; Sayles *et al.*, 1970). The porosity value used in this correction was derived by averaging the GRAPE values over an interval of 15 centimeters centered on the mid-point of each gamma count reading. The length of this interval is not meant to imply the effective length of core over which gamma counts are measured, but was chosen for its convenience in the computations. Hence the gamma counts presented here are solely measures of the natural gamma radiation of the minerals in each core. All values are plotted in the Core Summaries while, for reasons of scale, each point on the Hole Summaries represents the average of a group of four points.

Measurements over watery parts of cores are included although mixing of sediment in such cases may lead to a poor approximation of *in situ* values. The first and last counts on each core section are often low, since the counter "senses" the ends of the section.

Compressional Wave Velocity, Acoustic Impedance and Mean Velocity Below Sea-Bed

Most of the aspects of compressional wave velocity measurements on board *Glomar Challenger* have been summarized by Boyce (1970). To stress the importance of these measurements on the interpretation of reflection profiling records, the mean acoustic impedance (velocity × density) of each section of core is plotted here on the Site Summaries. The reflection coefficient for plane waves at vertical incidence is a simple function of the impedances of the material on either side of a reflecting boundary. A full understanding of reflectors seen on profiling records can only be achieved by computing synthetic seismograms from continuous downhole impedance data (Grant and West, 1965; Wuenschel, 1960).

The velocities measured at 400 kHz on board *Glomar Challenger* and plotted in this volume were determined at the pressure and temperature of the laboratory. Measurements were made at least four hours after the time a core was brought on deck to allow the core to approach the ambient temperature; the accuracy of the measurements (±1 m/sec) did not permit the detection of further velocity changes, due to approaching the ambient temperature, after four hours. The laboratory temperature varied over the range 19.5 to 25.5°C, sufficient to cause velocity changes of 16 m/sec in sea-water (Wilson, 1960). It is possible to apply velocity corrections from Wilson's tables so as to reduce all measurements to one temperature, but the validity of doing this for medium porosity sediments—with velocities mostly greater than that of sea-water—is in doubt although a similar method has been successfully used on surficial deep-sea sediments (Hamilton, 1963). It seems best to assume, with small error, that all measurements were taken at the median temperature of 23°C.

The occasional ellipticity of some core liners (Boyce, 1970) will introduce a random error into the measurements. More seriously a systematic error will be present due to some cores not occupying all the space inside the liner. With "soft" cores there is invariably a watery layer of smeared sediment several millimeters thick at the contact of the core and liner possibly causing a systematically low velocity to be obtained. "Hard" cores, on the other hand, tend to have diameters appreciably less than the core liner. A different method of measuring velocity was introduced for these cores during Leg 12. The space remaining in the liner was filled with sea-water and the travel time difference relative to the reference sample was measured in the normal way. The core diameter at each measurement point was then measured with a Vernier rule and this figure was used in the velocity calculation.

All velocity data are plotted on both Core and Site Summaries. Mean velocities between the sea-bed and the deepest reflector have been calculated at most sites on the basis of qualitative correlations between the acoustic impedance curves, drilling characteristics and the reflectors observed on the reflection profiling records obtained at each site (see Chapters 3 to 10). These data can be used to check the laboratory measurements of velocity if mean velocities are derived from the latter, and they indicate that the correction for all sources of systematic error (to be applied to the laboratory measurements) is +(0.20 ± 0.06) kms/sec for measurements on cores from 500 meters downhole (see also Chapter 12). This correction will be mostly due to the changes in temperature, hydrostatic pressure and overburden pressure which the core has experienced, but probably also includes the disturbing effect of the coring process which may tend to break up the grain-to-grain bonding in the sediment with a consequent reduction in rigidity and bulk modulus and, hence, sediment velocity. The discrepancy has the wrong sign for it to be explained as the result of transverse anisotropy of the sediment (for example, Hamilton, 1970), but it may be possible to explain away at least some of it by body wave dispersion due to the frequencies of the two measurements differing by 4 orders of magnitude (Hamilton *et al.*, 1970).

Penetrometer

This instrument has been described in detail by the American Society of Testing and Materials (1965) and briefly by Boyce (1970). It was intended to measure the relative load bearing strengths of the sediment cores, however it should be noted that, in general, penetration is parallel to bedding planes, not normal to them. In a general way the penetrometer measurements relate to the qualitative expressions used in the visual core descriptions such as "firm", "hard", "soft", etc., and could perhaps be used to set up a more stringent set of phrases for describing core firmness. Since the penetrometer values cover a wide range yet show only slightly varying small values in the lower parts of most holes, they are displayed here on a logarithmic scale.

Two sizes of needle were used with the instrument and the size of needle used at each site is listed in Table 2.

TABLE 2
Use of Penetrometer Needles

Site	111	112	113	114	115	116	117	118	119
Needle Diameter (mm)	1	2	2	2?	–	2	1	1	1

Sediment Density, Porosity and Water Content

The density of the sea-water saturated cores was measured in three ways on board ship.

(1) The first method was to weigh each full core section and this yielded a bulk density for the whole 1.5-meter long section. These values may be systematically slightly low because of the watery or void parts of some sections which were not allowed for (see next section). These data are plotted on the Core Summaries only, at the mid-depth of the appropriate section.

(2) The second set of density measurements was obtained during the measurement of water content on 0.5 cc cylindrical samples taken from the cores with adapted graduated syringes. These measurements are subject to an estimated 10 per cent error in the sample volume which is determined from the graduations on the syringe, and hence the density may be in error by up to 0.20 gm/cc (see next section). These data are not plotted on the Core and Hole summaries but are compared with other density measurements below.

(3) The last set of density measurements was composed of continuous values obtained along the length of each core with the Gamma-Ray Attenuation Porosity Evaluator (GRAPE). The GRAPE method is described in detail by Evans and Cotterell (1970). Essentially the number of electrons in the scanned volume of core is measured, and this figure is related to true density by a factor, the Compton mass attenuation coefficient (μ), which is constant (within ±1 per cent) for most common minerals. Montmorillonite, chlorite, pyrite, orthoclase, albite and some evaporite products are among those few minerals for which μ is significantly different, and sediments containing appreciable quantities of these minerals will be given low densities by GRAPE. Similarly, and more importantly, water and brine have mass attenuation coefficients which are 9 to 10 per cent greater than that of quartz, and this can cause errors in the density determinations for water-saturated sediments with large porosities (Brier *et al.*, 1969; Corey and Hayes, 1970). For instance a core with 80 per cent porosity will apparently have a density 6 per cent (0.10 gm/cc) greater than its true value if no correction is made.

Neglecting the errors in the GRAPE densities for the moment, it is clear that if the cores are assumed to be a two component mixture of sea-water and mineral grains of a single density, the core porosity can be calculated if the sea density and mineral density are known. A +6 per cent error in sediment density causes a −3.5 per cent error in the derived porosity. Similarly for an 80 per cent porosity sediment, an error of +0.1 gm/cc in the assumed grain density will give only a −1.3 per cent error in the calculated porosity. Therefore all the GRAPE porosity values displayed in this volume have been calculated for a single grain density of 2.67 gm/cc and a water density of 1.024 gm/cc. If the reader wishes to calculate the porosity applicable to a different grain density he may do so using Figure 8, however he should bear in mind that the repeatability of a similar GRAPE instrument has been shown to be within 3 per cent porosity (Harms and Choquette, 1965).

An iterative procedure, allowing for the large μ of water, can be used however to arrive at an accurate determination of density and porosity. Starting with the μ value applicable to most sedimentary minerals (0.100 for a Ba^{133} 0.3–0.36 MeV source), the first estimate of the bulk density of the saturated sediment is made by linear interpolation between the densities the water and aluminum standards would have if their Compton mass attenuation coefficients were 0.100. These values are 1.125 (calculated from a μ for water of 0.1099 cm^2/gm) and 2.60 gm/cc (Anonymous, 1966), respectively. The density value allows an estimate of the water content (assuming values for the water and grain densities) which in turn can be used to calculate a more realistic value of μ for the sediment, hence a better density estimate is obtained, and so on (Whitmarsh, 1971). The μ for sea-water is taken as 0.1099 cm^2/gm in these calculations. Although the calculated sediment density obtained by this method is dependent on the assumed grain density, choosing grain densitities of 2.5 and 2.9 gm/cc will only yield a density difference of up to 0.015 gm/cc for normal sediments. Porosity is calculated from the final

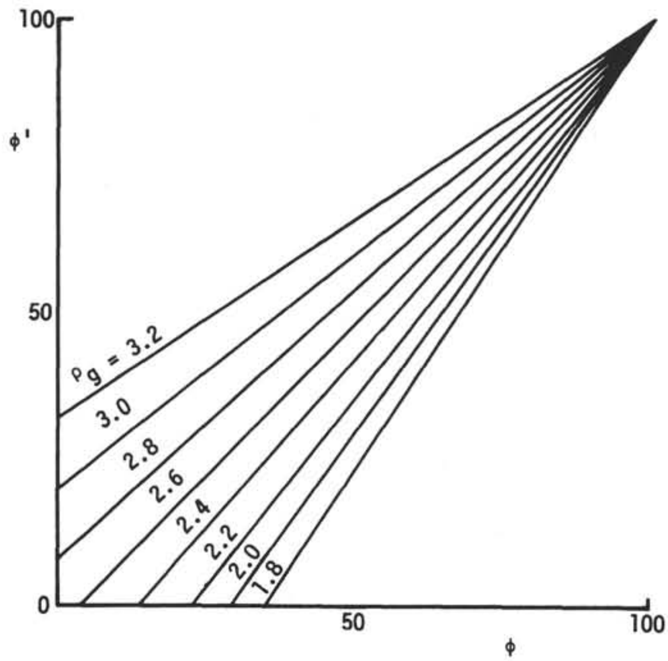

Figure 8. *Graph for determining porosity (ϕ) for grain densities (ρ_g) other than 2.67 gm/cc by using the displayed GRAPE porosity (ϕ) which is based on a 2.67 gm/cc grain density.*

density estimate using assumed water and grain densities in the usual way. This is the procedure which led to the values plotted in this volume. On previous legs of the Deep-Sea Drilling Project, the GRAPE densities were calculated by linear interpolation between standard densities of 1.024 or 1.03 and 2.60 gm/cc. In principle this is only correct if the Compton mass attenuation coefficient of the whole sediment varies linearly with bulk density over the range of the standard densities. This is not so because μ varies linearly with water content which in turn varies as the *inverse* of bulk density. In practice a small systematic error of up to 0.004 gm/cc seems to have been introduced by the former method.

In the Core Summaries the GRAPE data have been averaged over 1 centimeter intervals before plotting, and over 20-centimeter intervals for the Site Summaries.

It is not advisable to calculate porosity values from the sediment densities derived from the water content measurements because of the large errors in these densities. Porosities can however be derived directly from the water contents if a sea-water density and a grain density are assumed but this has not been done here (however, see next section).

Water content is defined as the percentage weight of water, driven off by heating to about 105°C, relative to the total weight of a sample. These values are accurate to better than 1 per cent.

Intercomparisons of Independent Sediment Density, Porosity and Water Content Measurements

To ascertain the reliability, or at least consistency, of the sediment density and porosity measurements intercomparisons were made of data obtained at sea by independent means. The opportunity did not arise to make precise comparative measurements on samples ashore, but this aspect has been investigated already by Gealy (1971).

The most significant comparison is that between the section densities and the GRAPE densities adjusted by the iterative procedure and averaged over a whole section. Straight lines were fitted by least squares to plots of these two parameters for each site individually and for all sites together. This procedure was also followed for plots of the unadjusted GRAPE densities (that is, those derived by interpolation between the 1.125 and 2.60 gm/cc densities of the standards alone) against the section densities. The results are presented in Table 3 and Figures 9 and 10. From the table it is clear that in the majority of cases a closer fit to the expected line was obtained after the GRAPE data were adjusted because A and B come closer to the expected values of 1.0 and zero, respectively. The fact remains however that all except two of the lines fitted to the adjusted GRAPE data have parameters A and B which are systematically less than and greater than the expected values, respectively. These values of A and B, and the plotted data in Figure 10 suggest that the fitted lines are being biased by a small number of low section densities which probably resulted from undetected or ignored void spaces in these sections. Consequently, the photographs of the split sections (where available) were checked for signs of such void spaces and all section densities measured over sections with voids were omitted. The line fitted to all the remaining data (Table 3, bottom line) has a slope even closer to 1.0 and an intercept of almost zero. This line differs by no more than 0.03 gm/cc from the expected line over the range of measured densities.

As a whole, therefore, the consistency of the adjusted GRAPE densities and the section densities is very good and lends strong support to the iterative method of adjusting the GRAPE data.

Bulk densities derived during the water content measurements and adjusted GRAPE densities were also compared. The closest GRAPE density value to the water content sample (within ±0.5 centimeter, chosen from a listing of GRAPE densities averaged over 1-centimeter intervals) was paired with each "water content" density. Straight lines were fitted by least squares to the data of each site and of all the sites together. The lines fitted by site all have large standard errors on their slope and intercept. The line fitted to all 103 data points (Figure 5) is,

$$Y = (0.776 \pm 0.060)X + (0.348 \pm 0.101)$$

where Y = "water content" density
X = adjusted GRAPE density

Admittedly this comparison is subject to mismatch errors, between the point from which the water content sample was obtained and the point at which the GRAPE measurement was made, due to sliding of the core within the liner. However the data used above were chosen with care and the mismatch error should be slight. Consequently, if one accepts the adjusted GRAPE data as correct, the "water content" densities appear to have a large random scatter lying within the range ±0.24 gm/cc of the expected values. The above fitted line hardly differs from that determined by Gealy (1971) from all her data,

$$Y = (0.786 \pm 0.025)X + (0.266 \pm 0.016)$$

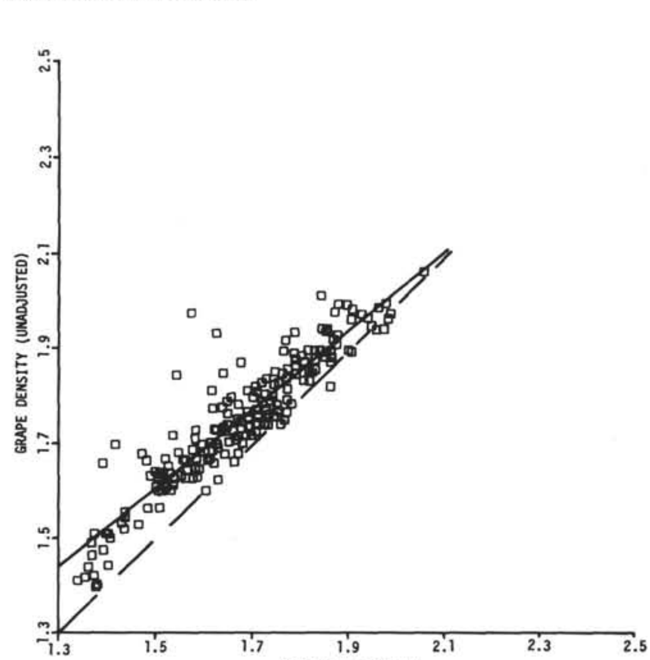

Figure 9. *Plot of section weight density against unadjusted GRAPE density averaged over a section. The continuous line is the line fitted by least squares, the dashed line is the 45° line.*

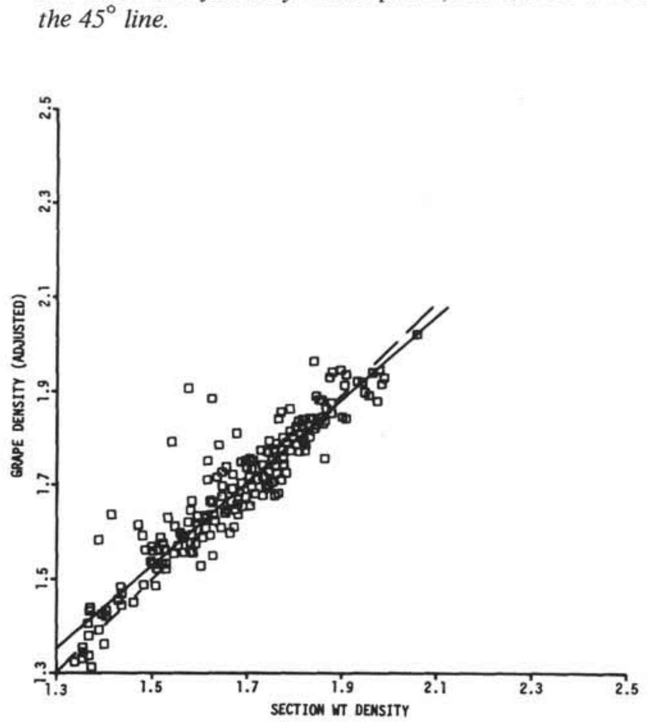

Figure 10. *Plot of section weight density against adjusted GRAPE density averaged over a section. The continuous line is the line fitted by least squares, the dashed line is the 45° line.*

The range of error determined from Figure 11 is close to that deduced from the expected error in determining the volume of the water content samples. Hence it is suggested that the "water content" densities have a large random error due to the inaccuracy in determining the sample volume.

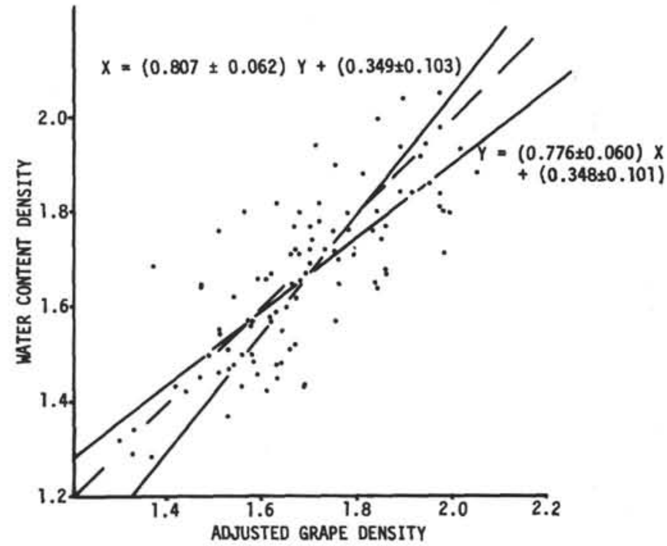

Figure 11. *Plot of sediment density derived from measurements made during the water content determination against the corresponding adjusted GRAPE density. The continuous lines are the lines fitted by least squares and the dashed line is the 45° line.*

Implicit in the method of least square fitting employed to obtain the above two equations is the assumption that the "water content" density is dependent on the GRAPE density. Clearly this is no more true than to say that the GRAPE density is dependent on the "water content" density since the two parameters are independent estimates of the same variable. Hence, we may assign the GRAPE density as the dependent variable and obtain the line (Figure 11),

$$X = (0.807 \pm 0.062)Y + (0.349 \pm 0.103)$$

This line differs considerably from the first fitted line because of the large scatter of the points in Figure 11. In Figure 11, the best estimate of the line following the trend of the points will lie between the two lines fitted above and pass through their point of intersection. Such a line will have a slope very close to unity and will lie about 0.03 gm/cc below the expected dashed line. This systematic difference may be barely significant but suggests that the "water content" densities are systematically low or the GRAPE densities systematically high by 0.03 gm/cc (or there is a combination of these factors).

Finally, it is also possible to check independently the validity of the GRAPE porosity values wherever a water content measurement was made. The reason for this is the relationship between porosity and water content,

$$\frac{1}{\phi} = \frac{\rho_W}{\rho_g} \times \frac{1}{W} + \left(1 - \frac{\rho_W}{\rho_g}\right)$$

where,

ϕ is the sediment porosity
W is the true water content (salt-free)
ρ_W is the water density
ρ_g is the grain density

Assuming $\rho_w = 1.024$ and $\rho_g = 2.67$ gm/cc, as used in the derivation of GRAPE porosities, the expected relation is,

$$\phi^{-1} = 0.384W^{-1} + 0.616$$

or

$$W^{-1} = 2.604\phi^{-1} - 1.604$$

The least squares fits obtained by pairing GRAPE porosity measurements with the 103 water content measurements were (Figure 12),

$$\phi^{-1} = (0.315 \pm 0.015)W^{-1} + (0.711 \pm 0.049)$$
$$W^{-1} = (2.595 \pm 0.122)\phi^{-1} - (1.261 \pm 0.213)$$

depending on which parameter is to be estimated from the other. These data will be subject to the same mismatch error as existed in the comparison of "water content" densities and GRAPE densities. In addition a small error of about −2 per cent in water content will be introduced by the fact that the calculated water content measurements are not derived on a salt-free basis but this is not allowed for here.

Applying the same statistical arguments as were used in discussing "water content" densities it is clear that the best trend line on Figure 12 will lie between the fitted lines and fall below the expected (dashed) line. Assuming that the water content measurements are without systematic error, we must explain why the GRAPE porosities are apparently too large. One explanation of this might be that the grain density assumed in the GRAPE porosity calculations is too small. An increase of grain density to 2.82 gm/cc would be sufficient to shift the mean of the plotted points up onto the expected (dashed) line, however this suggestion is incompatible with the mean grain density of 2.45 gm/cc calculated from all the water content samples. Even allowing for the possible systematic error in "water content" density the mean grain density could not exceed 2.52 gm/cc. The real explanation probably lies in the sediment on which the two measurements of GRAPE porosity and water content are made. The water content sample does not contain any of the smeared watery sediment which exists around the circumference of the core, while the volume sampled by the GRAPE instrument does include this smeared sediment. This explanation is borne out by the distribution of points in Figure 12, since only eight points indicate a porosity appreciably less than that expected from the measured water content. Even more striking is the apparently single-tailed normal distribution of the residuals, from the expected line, of points falling below the expected line suggesting that the smeared sediment randomly causes the GRAPE porosity values to be higher than the best estimate of the porosity of the unsmeared sediment. The presence of chlorite and uncollapsed montmorillonite in appreciable amounts will add to the error in GRAPE porosity as explained above.

In conclusion, therefore, the results of the above comparisons can be summarized as follows,

(1) Section weight densities and mean GRAPE bulk densities for a section agree very well. Slight biasing of the section weight data towards lower values exists due to undetected or unallowed for voids. Both density determinations include the effect of smeared sediments around the

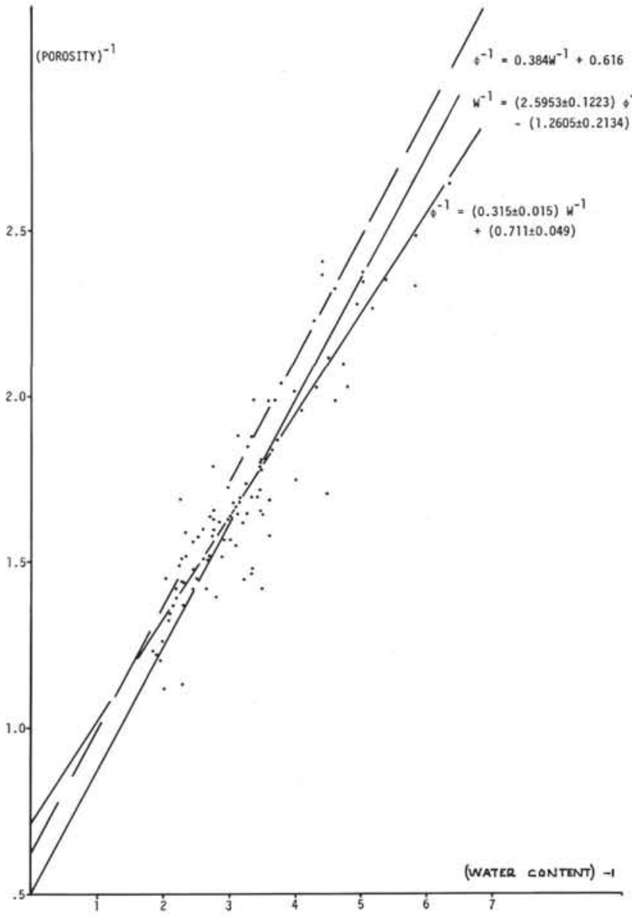

Figure 12. *Plot of (GRAPE porosity)*$^{-1}$ *against (water content)*$^{-1}$*: The two continuous lines are fitted by least squares, the dashed line is the expected relationship for a sediment composed of 1.024 gm/cc water and 2.67 gm/cc grains.*

core circumference and as estimates of the density of the unsmeared sediment may be systematically slightly low (probably rarely more than 5 per cent). As far as can be determined, the iterative method of deriving GRAPE densities is correct.

(2) Sediment densities derived from the mass and volume of the water content sample have a large random error (within the range ±0.24 gm/cc) due to the inaccuracy in determining the sample volume.

(3) The GRAPE porosity is normally greater than the porosity expected from the water content determination due to the GRAPE instrument including smeared watery sediment in the sampled volume. As an estimate of the porosity of the unsmeared sediment, the GRAPE value is therefore believed to be usually slightly high (probably rarely more than 5 per cent).

Notes on the Core and Site Summary Plots and their Description

Numbers have been used on the left of the Core Summary plots to indicate the degree of disturbance of the cores. Each number corresponds to a single class of disturbance. A key is given in Figure 13.

DISTURB. CLASS.	CHARACTER OF CORE
1	Void, empty, partly filled
2	Watery, sloppy, soupy Disrupted, drilling breccia, unsplit
3	Disturbed, various signs of plastic deformation
4	No sign of deformation

Figure 13. *Key to numbers used on the core summary plots to indicate disturbance of the cores.*

The GRAPE density and porosity traces often indicate the ends of sections, or voids within a core, by a steep slope to the left. These artifacts have been mostly removed from the Core Summary plots. The natural gamma counts similarly indicate the ends of sections on occasion by having low values. Because this effect is not always present the occasional low values have not been removed from the Core Summary plots.

The tops of the figures representing carbonate content and grain size proportions are drawn at the depth of the sample on which the measurement was made.

On the Site Summary plots the "end of section" effects tend to be accentuated on the GRAPE traces due to the averaging method and scale employed. Therefore, when using these plots the maximum density value (or minimum porosity) is usually the correct value for a particular section.

In the description of the physical properties for each site, porosity and water content are not usually mentioned. This is because the remarks about density are always directly applicable to porosity and water content provided one is aware that as density increases porosity and water content decrease and *vice versa*.

Consolidation of Sediments and Sedimentation Rates

An estimate of sediment consolidation is required in order to make corrections to sedimentation rates derived from paleontologically dated horizons at various depths down each hole. Sediment density, on average, increases with depth. If it is assumed that the increase is due solely to natural consolidation of the sediments then the degree of consolidation may be calculated. Factors which also affect sediment density and which may invalidate this assumption are,

(1) changes in grain size
(2) precipitation of mineral matter in pore spaces
(3) gross changes in grain density

If density increases linearly with depth it can be shown that the fractional shortening, due to consolidation, of the sediment column between the sea-bed and a depth (h) is S_h where,

$$S_h = \frac{\gamma}{\rho_o - \rho_w + \frac{dh}{2}} = 1 - C_h$$

where

ρ_o is the sediment density at the sea-bed
ρ_w is the sea-water density
d is the density gradient
C_h is the compaction of the sediment column

It follows that the fractional shortening between the two depths a and b, to which ages may have been assigned, is $S_{a,b}$ where,

$$S_{a,b} = \frac{b - a}{\frac{b}{S_b} - \frac{a}{S_a}}$$

TABLE 3

Site	Adjusted GRAPE Densities		Unadjusted GRAPE Densities		Number of Points
	A	B	A	B	
111	0.877 ± 0.030	0.216 ± 0.054	0.823 ± 0.028	0.369 ± 0.050	34
112	0.933 ± 0.036	0.103 ± 0.058	0.886 ± 0.036	0.249 ± 0.057	47
113	1.112 ± 0.059	−0.138 ± 0.100	1.045 ± 0.057	0.038 ± 0.097	12
115	0.690 ± 0.162	0.640 ± 0.239	0.638 ± 0.091	0.785 ± 0.134	3
116	0.774 ± 0.054	0.373 ± 0.088	0.728 ± 0.051	0.514 ± 0.084	68
117	1.561 ± 1.378	−0.762 ± 2.171	1.460 ± 1.343	−0.536 ± 2.115	8
118	0.910 ± 0.099	0.191 ± 0.174	0.872 ± 0.100	0.319 ± 0.176	13
119	0.810 ± 0.053	0.348 ± 0.093	0.738 ± 0.053	0.533 ± 0.092	48
ALL	0.896 ± 0.024	0.189 ± 0.030	0.840 ± 0.023	0.346 ± 0.038	233
ALL*	0.938 ± 0.017	0.107 ± 0.028	–	–	208

Parameters A and B, with their standard errors, of Y on X least squares regression line Y = AX + B, where Y = GRAPE density averaged over a section, X = section density, * indicates some poor data omitted, see text.

Tables of depths and shortening factors for different density gradients were calculated using $\rho_W = 1.024$ and $\rho_O = 1.45$ gm/cc, and these tables were used to correct the sedimentation rates for the effects of sediment consolidation.

DATA PRESENTATION

Nearly all the primary data concerning each site is presented in the chapter on the site whether processed on board or ashore. The sections of each site chapter in general have the following sequence:

Site background and objectives.
Survey data.
Drilling operations and list of cores cut.
Lithology.
Physical properties.
Paleontology and Biostratigraphy.
Sedimentation rates.
Discussion.
References.
Appendices:
  Smear slide observations.
  Grain size determinations.
  Carbon-carbonate determinations.
  Foraminiferal faunal list.
  Coccolith species lists.

At the end of each site chapter there are graphical summaries of the physical properties, lithology, biostratigraphy, etc. of each core on a scale of 9 meters per pair of facing pages.

Core photographs are next illustrated at a scale of 1.5 meters per page length, the six sections of a core being displayed on one page.

These are followed by graphical summaries of the physical properties, lithology, stratigraphic division etc. of each hole on a scale of 250 meters per pair of facing pages.

REFERENCES

Adams, J. A. S., 1962. Radioactivity of the lithosphere, **in** *Nuclear Radiation in Geophysics*. H. Israel and A. Krebs (Eds.), Berlin (Springer-Verlag), 1-17.

American Society of Testing and Materials, 1965. Standard method of test for penetration of bituminous material. *ASTM*. Designation D-5-65, 1007.

Amin, B. S., Kharkar, D. P. and Lal, D., 1966. Cosmogenic ^{10}Be and ^{26}Al in marine sediments. *Deep-Sea Res.* **13**, 805.

Anonymous, 1966. The Formation Density Log, in Schlumberger Log Interpretation Principles, 47-49.

Barsukov, O. A., Blinova, N. M., Vybornykh, S. F., Gulin, Yu. A., Dakhnov, V. N., Larionov, V. V. and Kholin A. I., 1964. *Radioactive Investigation of Oil and Gas Wells*. J. O. H. Muhlhaus (Transl.), N. Rast (Ed.). London (Pergamon Press), 299 pp.

Berggren, W. A., 1971. A Cenozoic time-scale: some implications for regional geology and biogeography. J. Foram. Res.., **1**.

Blow, W. H., 1969. Late Middle Eocene to Recent planktonic foraminiferal biostratigraphy. *Proc. First Intern. Conf. Plank. Microfossils*. E. J. Brill *Leiden* **1**, 199, 54 pls.

Boyce, R. E., 1970. **in** Maxwell *et al.*, 1970. *Initial Reports of the Deep Sea Drilling Project, Volume III*. Washington (U.S. Government Printing Office) 22 *et seq*.

Brier, C., Bennin, R. and Rona, P. A., 1969. Preliminary evaluation of a core scintillation counter for bulk density measurement in marine sediment cores. *J. Sediment. Petrol.* **39** (4), 1509.

Broecker, W. S., 1963. A preliminary evaluation of uranium series inequilibrium as a tool for absolute age measurement on marine carbonates. *J. Geophys. Res.* **68** (9), 2817.

Corey, J. C. and Hayes D. W., 1970. Determination of density and water content of marine sediment in an unextruded core using fast neutron and gamma-ray attenuation. *Deep-Sea Res.* **17**, 917.

Evans, H. B., Lucia, J. A., 1970. Natural gamma radiation scanner. **In** Peterson *et al.*, 1970. *Initial Reports of the Deep Sea Drilling Project, Volume II* (U.S. Government Printing Office) 458.

Evans, H. B. and Cotterel, C. H. 1970. Gamma ray attenuation density scanner. **In** Peterson *et al.*, 1970, *Initial Reports of the Deep Sea Drilling Project, Volume II.* Washington (U.S. Government Printing Office) 460.

Gealy, E. L., 1971, Saturated bulk density; grain density and porosity and sediment cores from the Western Equatorial Pacific: Leg 7, *Glomar Challenger.* **In** Winterer *et al.*, 1971. *Initial Reports of the Deep Sea Drilling Project, Volume VII*. Washington (U.S. Government Printing Office) 1081.

Grant, F. S. and West, G. F., 1965. *Interpretation Theory in Applied Geophysics*. (McGraw-Hill), 583 pp.

Hamilton, E. L., 1963. Sediment sound velocity measurements made *in situ* from bathyscaph Trieste. *J. Geophys. Res.* **68**, 5991.

Hamilton, E .L., Bucker, H. O., Keir, D. L. and Whitney, J. A., 1970. Velocities of compressional and shear waves in marine sediments determined *in situ* from a research submersible. *J. Geophys. Res.* **75**, 4039.

Hamilton, E. L., 1970. Sound velocity and related physical properties of marine sediments, North Pacific. *J. Geophys. Res.* **75**, 4423.

Harms, J. C. and Choquette P. W., 1965. Geologic evaluation of a gamma-ray porosity device, *Trans. 6th Annual SPWLA Logging Symp.* **2**, C1-C37.

Hinte, J. E. van, 1971. The Cretaceous time-scale and planktonic foraminiferal zones. *Proc. Koninkl. Ned. Akad. Wetenschap. Amsterdam.* Ser. B, **74**, 1 textfigure.

Koczy, F. F. and Rosholt, J. N., 1962. Radioactivity in oceanography. **In** *Nuclear Radiation in Geophysics*. H. Israel and A. Krebs (Eds.) Berlin (Springer-Verlag), 18.

Krumbein, W. C. and Pettijohn, F. J., 1938. *Manual of Sedimentary Petrography*. New York (Appleton-Century).

Lederer, C. M., Hollander, J. M. and Pearlman, I., 1967. *Table of Isotopes*. (John Wiley and Sons Inc), 594 pp.

Martini, E., 1970. Standard Palaeogene calcareous nannoplankton zonation. *Nature*. **226** (5245), 560.

Martini, E. and Worsley, T., 1970. Standard Neogene calcareous nannoplankton zonation. *Nature.* **225** (5229), 289.

Matthews, D. J. 1939. Tables of the velocity of sound in pure water and in sea water. *Hydrographic Dept., Admiralty. London*. HD282.

Olausson, E. 1960. Description of sediment cores from Central and Western Pacific with the adjacent Indonesian region. *Rep. Swedish Deep Sea Exped.* **6** (5), 161.

Pettijohn, F. J. 1957. *Sedimentary Rocks.* New York (Harper Bros.).

Picciotto E. and Wilgain, S., 1954. Thorium determination in deep-sea sediments. *Nature.* **173**, 623.

Prospero, J. M. and Koczy, F. F., 1966. Radionuclides in oceans and sediments. **In** *Encyclopaedia of Oceanography.* R. W. Fairbridge (Ed.), New York (Reinhold Publ. Corp.), 730 pp.

Richards, A. F., 1962. Investigations of seep-sea sediment cores, II. Mass physical properties. *Tech. Rept. 106, U.S. Navy Hydrog. Office.* 146 pp.

Sayles, F. L., Manheim, F. T. and Chan, K. M., 1970. Interstitial water studies on small core samples, Leg 4. **In** Bader *et al.*, 1970, *Initial Reports of the Deep Sea Drilling Project Volume IV.* Washington (U.S. Government Printing Off.) 401.

Tatsumoto, M. and Goldberg, E.D., 1959. **In** *Geochim. Cosmochim. Acta.* **17**, 201.

Wasson, J. T., 1963. Radioactivity in interplanetary dust. *Icarus.* **2**, 54.

Whitmarsh, R. B., 1971. Precise sediment density determination by gamma-ray attenuation alone. *J. Sediment. Petrol.* **41**, 882.

Wilson, W. D., 1960. Speed of sound in sea water as a function of temperature, pressure, and salinity. *J. Acoust. Soc. Am.* **32**, 641.

Wuenschel, P. C., 1960. Seismogram synthesis including multiples and transmission coefficients. *Geophys.* **23**, 106.

PLATE 1

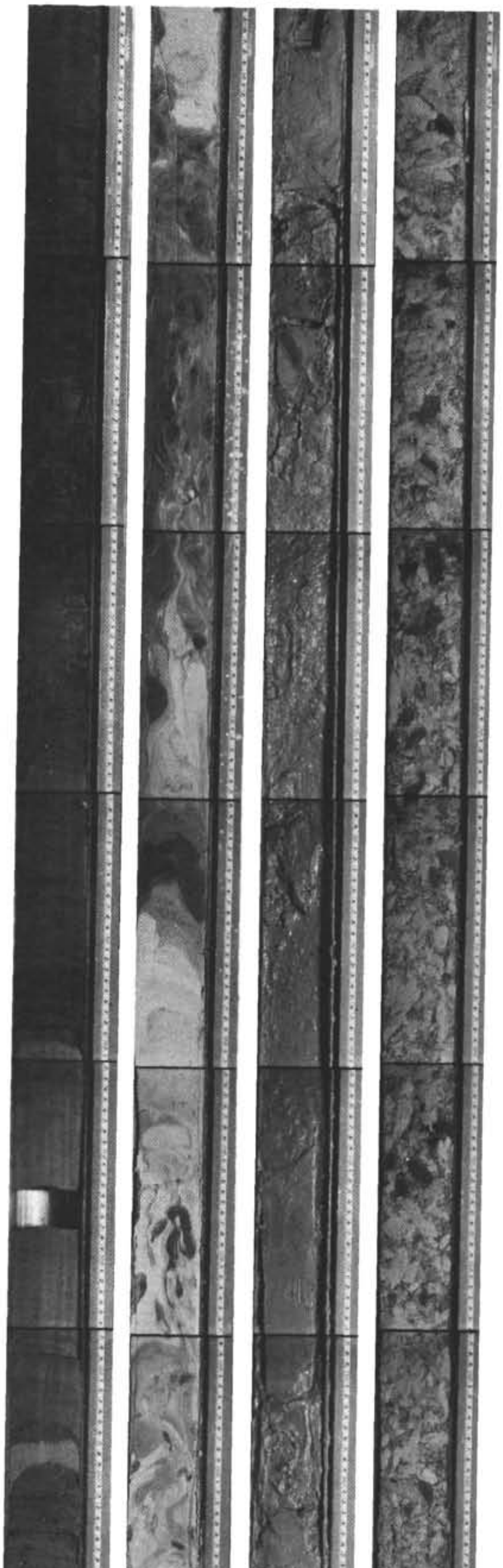

Degrees of drilling disturbance, (a) slight bending of bedding planes (111-3-3), (b) extreme bending of bedding planes (116A-4-5), (c) a watery core (112-1-6), (d) a drilling breccia (111A-7-3).